

# The correlation discrete variable representation revisited

Uwe Manthe\*

*Theoretische Chemie, Fakultät für Chemie, Universität Bielefeld,  
Universitätsstr. 25, D-33615 Bielefeld, Germany*

(Dated: April 6, 2026)

The correlation discrete variable representation (CDVR) enables efficient quantum dynamics calculation with the multi-layer multi-configurational time-dependent Hartree (MCTDH) approach on general potential energy surfaces. It employs a time-dependent quadrature to compute potential energy matrix elements, thereby eliminating the need to refit the potential to a sum of products form. The non-hierarchical CDVR conserves the inherent symmetry properties of tree-shaped wavefunction representations and drastically reduces the number of grid points compared to the original hierarchical CDVR. However, it requires projection on the space spanned by the single-hole functions (SHFs) at each node of the tree, which can introduce unphysical couplings for unconverged basis sets. In this work, the non-hierarchical CDVR is revisited and a revised approach that avoids explicit projection on the single-hole space is introduced. The computational costs of the revised approach scale favorably with the number of single-particle functions (SPFs): for a tree with three edges at each node and  $n$  SPFs at each edge, a  $n^4$  scaling is achieved. Furthermore, a revised scheme that uses artificial SPFs to systematically increase the accuracy of the CDVR quadrature is presented. Computations studying the photodissociation of NOCl, the vibrational states of methyl, and the non-adiabatic quantum dynamics of photoexcited pyrazine demonstrate the accuracy and efficiency of the revised non-hierarchical CDVR. Notably, for the 24-dimensional pyrazine system the use of the CDVR does not increase the required CPU time compared to calculations utilizing the sum of products form of the vibronic coupling model.

\* Author to whom correspondence should be addressed:  
uwe.manthe@uni-bielefeld.de

## I. INTRODUCTION

The (multi-layer) multi-configurational time-dependent Hartree (MCTDH) approach<sup>1-4</sup> utilizes tensor contraction to enable accurate high-dimensional quantum dynamics calculation. It has been used by many researchers to study a large variety of systems.<sup>5-29</sup> High-dimensional MCTDH calculations on detailed full-dimensional potential energy surfaces (PES) studied, e.g., reactions of methane with atoms,<sup>30-44</sup> proton transfer in malonaldehyde,<sup>45-50</sup> or large amplitude motion in the Zundel and Eigen cations.<sup>51-57</sup> Benchmark MCTDH simulations based on high-dimensional model Hamiltonians investigated the non-adiabatic dynamics in pyrazine<sup>58-60</sup> and the electron transfer and transport in the condensed phase<sup>3,61-63</sup>. Further examples can be found in various reviews on the subject (see, e.g., Refs. 64-71).

The representation of the Hamiltonian is an important aspect in any quantum dynamics method using tensor contraction. An efficient implementation of the MCTDH approach can be straightforwardly achieved for Hamiltonians that can be written as a sum of products (SOP) of operators acting only on a single degree of freedom. The SOP form was intensively used in early work utilizing the (single-layer) MCTDH approach.<sup>2,64</sup> In multi-layer MCTDH calculations, matrix elements of SOP Hamiltonians can be recursively calculated using successive bottom up and to down sweeps.<sup>4</sup>

Studying the quantum dynamics on accurate ab initio PESs poses another challenge. These PESs typically do not show a SOP form. Different strategies have been devised to address the issue. Meyer and co-workers<sup>72-77</sup> developed techniques to refit the PES in the SOP form required by the standard MCTDH implementation. They successfully used this approach to study malonaldehyde<sup>48,50</sup> and the Zundel and Eigen cations<sup>51-57</sup>. Alternatively, grid-based schemes can be used to directly compute potential energy matrix elements without refitting the PES. The correlation discrete variable representation (CDVR)<sup>4,78-81</sup> employs a time-dependent quadrature to efficiently compute all potential energy matrix elements appearing in the MCTDH equations of motion. This approach was successfully used, e.g., to study the reaction of methane with different atoms<sup>30-43,82-87</sup> or to compute the tunneling splittings in the ground and vibrationally excited states of malonaldehyde.<sup>45-47,49</sup> The collocation scheme of Wodraszka and Carrington<sup>88-91</sup> offers an alternative grid-based approach facilitating MCTDH calculations on general potential energy surfaces.

The original CDVR approach<sup>78</sup> designed for single MCTDH calculations can be viewed as a two-layer Smolyak<sup>92-94</sup> quadrature. At the top layer, a sparse grid accounting for correlation effects is built based on time-dependent discrete variable representations (DVRs) associated with the single-particle functions (SPFs). On the second layer, finer grids increase the grid's density in

a single direction using the respective time-independent DVR points. This design scheme can be extended to a multi-layer MCTDH/CDVR approach.<sup>4</sup> It employs increasingly large grids at lower layers of the multi-layered tree representation and thus is called hierarchical CDVR in the following.

Progress in recent MCTDH method development took advantage of a symmetric, non-hierarchical view on the multi-layer MCTDH wavefunction. By altering the choice of the root node, the role of SPFs and single-hole functions (SHF) in the MCTDH formalism can be interchanged and different equivalent multi-layer MCTDH representation can be obtained.<sup>95–97</sup> Based on these ideas, a non-hierarchical CDVR approach has been introduced.<sup>98,99</sup> The approach employs a revised grid design that uses roughly equal numbers of grid point at all layers of the tree. Total number of grid points is significantly decreased compared to the original hierarchical CDVR and roughly equals the total number of expansion coefficients used in the MCTDH wavefunction representation.

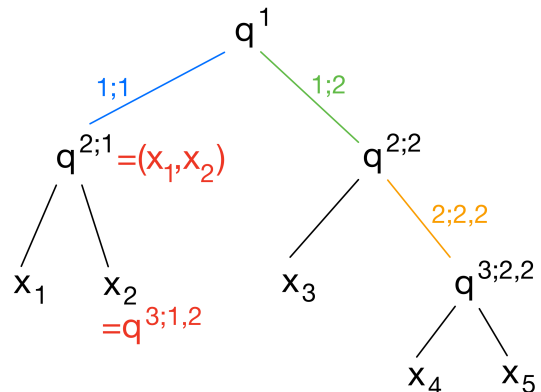
The non-hierarchical CDVR introduced in Refs. 98,99 requires projection onto the space spanned by the SHF to obtain edge-based potential corrections. This projection introduces undesirable features.<sup>99</sup> First, the CDVR potential operator can affect even parts of the wavefunction that depend on coordinates not present in potential function. This unphysical behavior only vanishes in the limit of a converged MCTDH wavefunction representation. Second, the CDVR scheme does not guarantee a correct description of separable potentials in case of an unconverged MCTDH wavefunction representation. Third, the calculation of the CDVR matrix elements scales less favorably than the application of the CDVR potential operator: for a node with  $f$  edges and  $n$  SPFs at each edge, the computational costs for the calculation of the CDVR matrix elements scale as  $n^{f+3}$  while the application of the CDVR potential operator exhibits a more favorable  $n^{f+1}$  scaling.

In the present work, a revised non-hierarchical CDVR is developed that avoids the projection onto the space spanned by the SHF and eliminates all the undesirable features mentioned above. The result scheme can be implemented with a numerical effort scaling as  $n^{f+1}$ .

Furthermore, a scheme to replace weakly occupied SPFs by artificial SPFs designed to increase the accuracy of CDVR quadrature is presented. This scheme is based upon the ideas outlined in Ref. 100 and enables numerically exact MCTDH/CDVR calculations that properly converge to the exact result with increasing SPF basis set size.

The article is organized as follows. The multi-layer MCTDH approach and the original non-hierarchical CDVR are briefly in Sects. II and III. Then the revised CDVR scheme is described in Sect. IV. Sect.V discusses the use of artificial SPFs to improve the accuracy of the CDVR quadrature. Numerical examples illustrate the accuracy and efficiency of the different schemes

FIG. 1: The multi-layer MCTDH approach: the grouping of physical coordinates  $x_i$  into logical coordinates  $\mathbf{q}^{l;\kappa_1, \dots, \kappa_{l-1}}$  and the labeling of nodes and edges are illustrated.



(Sect.VI): the photodissociation of NOCl (3D), the vibrational states of methyl (6D), and the  $S_0 \rightarrow S_2$  excitation in pyrazine (24D) are studied. Finally, conclusions and an outlook are given in Sect.VII.

## II. THE MULTI-LAYER MCTDH APPROACH

The multi-layer MCTDH approach<sup>1–4</sup> employs a tree-shaped structure to represent the system's wavefunction. As illustrated in Fig.1, the physical coordinates  $x_1, x_2, \dots, x_f$  are grouped into sets of logical coordinates  $\mathbf{q}^{l;\kappa_1, \dots, \kappa_{l-1}}$  where the superscripts ( $l; \kappa_1, \dots, \kappa_{l-1}$ ) indicate the specific node and  $l$  is the number of the layer. An edge connecting the nodes ( $l; \kappa_1, \dots, \kappa_{l-1}$ ) and ( $l+1; \kappa_1, \dots, \kappa_l$ ) is denoted by ( $l; \kappa_1, \dots, \kappa_l$ ) (see the colored labels in Fig.1).

Starting from the root node of the tree, the system's wavefunction  $\Psi(x_1, \dots, x_f, t)$  is expanded in orthonormal sets of SPFs that can be associated with the  $\nu$  edges ( $1; \kappa$ ) connecting the root node with its children:

$$\Psi(x_1, \dots, x_f, t) = \sum_{j_1, \dots, j_\nu} A_{j_1, \dots, j_\nu}^1(t) \prod_{\kappa=1}^{\nu} \phi_{j_\kappa}^{1;\kappa}(\mathbf{q}^{2,\kappa}, t). \quad (1)$$

The SPFs are defined recursively. The orthonormal set of SPFs  $\phi_n^{l;\kappa_1, \dots, \kappa_l}(\mathbf{q}^{l+1;\kappa_1, \dots, \kappa_l}, t)$  at the edge ( $l; \kappa_1, \dots, \kappa_l$ ) is obtained from the SPFs at the lower-layer edges ( $l+1; \kappa_1, \dots, \kappa_l, \kappa_{l+1}$ ):

$$\phi_n^{l;\kappa_1, \dots, \kappa_l} = \sum_{j_1, \dots, j_\nu} A_{n; j_1, \dots, j_\nu}^{l+1;\kappa_1, \dots, \kappa_l} \prod_{\kappa=1}^{\nu} \phi_{j_\kappa}^{l+1;\kappa_1, \dots, \kappa_l, \kappa}. \quad (2)$$

Here the  $A^{l+1;\kappa_1, \dots, \kappa_l}$  denotes expansion coefficients and  $\nu$  is the number of edges connecting the node ( $l; \kappa_1, \dots, \kappa_{l-1}$ ) to nodes ( $l+1; \kappa_1, \dots, \kappa_l$ ) of the lower layer. At the bottom layer of the tree, the SPFs are replaced by time-independent basis functions  $\chi_n^\kappa$ .

In the above description, all nodes and edges are labeled according to their absolute position in the given

tree. These labels specify the positions relative to the chosen root node. However, the definitions of all objects appearing in the above description only refer to neighboring nodes and edges. Thus, the relative position in the tree play a central role. To address nodes and edge via their relative position, an alternative notation specifying the neighborhood of an arbitrarily chosen reference node  $(\lambda) = (l; \kappa_1, \dots, \kappa_{l-1})$  is used.<sup>99</sup> Nodes connected to  $(\lambda)$  are denoted as  $(\lambda \circ j)$ :  $(\lambda \circ 0)$  refers to the node  $(l-1; \kappa_1, \dots, \kappa_{l-2})$  directly above  $\lambda$  while  $(\lambda \circ \kappa)$  with  $\kappa > 0$  refers to a lower node  $(l+1; \kappa_1, \dots, \kappa_{l-1}, \kappa)$ . An edge connecting the nodes  $(\lambda)$  and  $(\lambda \circ \kappa)$  can be denoted either by  $(\lambda|\lambda \circ \kappa)$  or by  $(\lambda \circ \kappa|\lambda)$ . Here the ordering allows one to distinguish directions:  $(\lambda|\nu)$  implies moving from node  $(\lambda)$  to node  $(\nu)$  while  $(\nu|\lambda)$  specifies the opposite direction. Using this notation, Eq.(2) can be rewritten as

$$\phi_n^{\lambda \circ 0|\lambda} = \sum_{j_1, \dots, j_\nu} A_{n; j_1, \dots, j_\nu}^\lambda \prod_{\kappa=1}^{\nu} \phi_{j_\kappa}^{\lambda|\lambda \circ \kappa}. \quad (3)$$

where a downward direction is used in the superscripts of the SPFs.

At any edge  $(\lambda|\lambda \circ \kappa)$ , the wavefunction can be decomposed in a sum of SPFs  $\phi_n^{\lambda|\lambda \circ \kappa}$  and single-hole functions (SHFs)  $\Psi_n^{\lambda|\lambda \circ \kappa}$ :

$$\Psi = \sum_n \phi_n^{\lambda|\lambda \circ \kappa} \cdot \Psi_n^{\lambda|\lambda \circ \kappa}. \quad (4)$$

The SHFs  $\Psi_n^{\lambda|\lambda \circ \kappa}$  depend on all coordinates not included in SPFs  $\phi_n^{\lambda|\lambda \circ \kappa}$ . Importantly, the SPFs and SHFs obey different normalization conditions:

$$\begin{aligned} \langle \phi_n^{\lambda|\lambda \circ \kappa} | \phi_m^{\lambda|\lambda \circ \kappa} \rangle &= \delta_{mn}, \\ \langle \Psi_n^{\lambda|\lambda \circ \kappa} | \Psi_m^{\lambda|\lambda \circ \kappa} \rangle &= \rho_{nm}^{\lambda|\lambda \circ \kappa}, \end{aligned} \quad (5)$$

where  $\rho^{\lambda|\lambda \circ \kappa}$  is the single-particle density matrix associated with the edge  $(\lambda|\lambda \circ \kappa)$ .

In the above description, a specific node was selected as root node and associated with the system's wavefunction (see Eq.(1)). However, only the tree's connectivity is important and the physical wavefunction is invariant with respect to the choice of the root node.<sup>96</sup> Altering the root node potentially exchanges the roles of SPFs and SHFs. Within the present notation, any change in the directionality of an edge affects the superscripts used in the SPFs and SHFs. Transformed SHFs and transformed SPFs as defined in Ref.97 can thus be denoted as SPFs and SHFs where the directionality in the superscript is inverted:<sup>99</sup>

$$\begin{aligned} \phi_n^{\lambda \circ \kappa|\lambda} &= \sum_k (\rho^{\lambda|\lambda \circ \kappa})_{kn}^{-\frac{1}{2}} \Psi_k^{\lambda|\lambda \circ \kappa}, \\ \Psi_n^{\lambda \circ \kappa|\lambda} &= \sum_k (\rho^{\lambda|\lambda \circ \kappa})_{nk}^{\frac{1}{2}} \phi_k^{\lambda|\lambda \circ \kappa}. \end{aligned} \quad (6)$$

Using this notation, the edge-based representation of the wavefunction takes the form

$$\begin{aligned} \Psi &= \sum_{n,m} \left( \rho^{\lambda|\lambda \circ \kappa} \right)_{nm}^{\frac{1}{2}} \cdot \phi_m^{\lambda \circ \kappa|\lambda} \cdot \phi_n^{\lambda|\lambda \circ \kappa}, \\ &= \sum_{n,m} \left( \rho^{\lambda \circ \kappa|\lambda} \right)_{nm}^{\frac{1}{2}} \cdot \phi_m^{\lambda|\lambda \circ \kappa} \cdot \phi_n^{\lambda \circ \kappa|\lambda}. \end{aligned} \quad (7)$$

Consequently,

$$\rho_{nm}^{\lambda|\lambda \circ \kappa} = \rho_{mn}^{\lambda \circ \kappa|\lambda}. \quad (8)$$

Defining the configurations  $\Phi_J^\lambda$  as

$$\Phi_J^\lambda = \prod_{\kappa} \phi_{j_\kappa}^{\lambda|\lambda \circ \kappa} \quad (9)$$

with  $\kappa = 0, \dots, \nu$  for non-root nodes and  $\kappa = 1, \dots, \nu$  for the root node, the wavefunction can be expanded in the basis of the configurations at any non-root node as

$$\begin{aligned} \Psi &= \sum_J \tilde{A}_J^\lambda \cdot \Phi_J^\lambda, \\ \tilde{A}_J^\lambda &= \sum_n (\rho^{\lambda \circ 0|\lambda})_{j_0 n}^{\frac{1}{2}} \cdot A_{n; j_1, \dots, j_\nu}^\lambda \end{aligned} \quad (10)$$

where the multi-index  $J = (j_0, j_1, \dots, j_\nu)$  is used.

The MCTDH equations of motion for the coefficients  $A_J^\lambda = A_{j_0; j_1, j_2, \dots}^\lambda$  then read<sup>99</sup> ( $\hat{H}$  is the system's Hamiltonian)

$$i \frac{\partial}{\partial t} A_J^\lambda = \langle \Phi_J^\lambda | \hat{H} | \Psi \rangle \quad (11)$$

if  $\lambda$  is the root node (with  $j_0 = 1$ ) and

$$\begin{aligned} i \frac{\partial}{\partial t} A_J^\lambda &= \left( 1 - \sum_m |\phi_m^{\lambda \circ 0|\lambda} \rangle \langle \phi_m^{\lambda \circ 0|\lambda} | \right) \\ &\cdot \sum_n (\rho^{\lambda \circ 0|\lambda})_{j_0 n}^{-\frac{1}{2}} \cdot \langle \Phi_{n, j_1, j_2, \dots}^\lambda | \hat{H} | \Psi \rangle \end{aligned} \quad (12)$$

if  $\lambda$  is a non-root node.

The matrix elements  $\langle \Phi_J^\lambda | \hat{H} | \Psi \rangle$  appearing in the equations of motion can be straightforwardly and efficiently computed for Hamiltonians  $\hat{H}_{SOP}$  showing a sum of products form<sup>1,4</sup>

$$\hat{H}_{SOP} = \sum_{t=1}^s c_t \cdot \prod_{k=1}^f \hat{h}_t^{prim;k} \quad (13)$$

where  $\hat{h}_t^{prim;k}$  denotes an operator acting only on the (primitive) coordinate  $x_k$ . Then at each node  $(\lambda)$  the terms  $\langle \Phi_J^\lambda | \hat{H} | \Psi \rangle$  appearing in the equations of motion

can be efficiently computed via

$$\begin{aligned} \langle \Phi_j^\lambda | \hat{H} | \Psi \rangle &= \sum_{t=1}^s c_t \cdot \sum_{i_0} \langle \phi_{j_0}^{\lambda|\lambda\circ 0} | \hat{h}_t^{\lambda;0} | \phi_{i_0}^{\lambda|\lambda\circ 0} \rangle \\ &\quad \cdot \sum_{i_1} \langle \phi_{j_1}^{\lambda|\lambda\circ 1} | \hat{h}_t^{\lambda;1} | \phi_{i_1}^{\lambda|\lambda\circ 1} \rangle \\ &\quad \cdot \dots \\ &\quad \cdot \sum_{i_\nu} \langle \phi_{j_\nu}^{\lambda|\lambda\circ \nu} | \hat{h}_t^{\lambda;\nu} | \phi_{i_\nu}^{\lambda|\lambda\circ \nu} \rangle \cdot \tilde{A}_{i_0, i_1, \dots, i_\nu}^\lambda. \end{aligned} \quad (14)$$

Here the operator  $\hat{h}_t^{\lambda;\kappa}$  is defined as the product of all operators  $\hat{h}_t^{prim;l}$  with  $x_l \in q^{\lambda\circ\kappa}$  for  $\kappa \neq 0$  or  $x_l \notin q^\lambda$  for  $\kappa = 0$ . All matrix elements  $\langle \phi_{j_\kappa}^{\lambda|\lambda\circ\kappa} | \hat{h}_t^{\lambda;\kappa} | \phi_{i_\kappa}^{\lambda|\lambda\circ\kappa} \rangle$  can be efficiently calculated using the recursive scheme described in Ref.4.

### III. NON-HIERARCHICAL MULTI-LAYER CDVR

The CDVR approach extends the type of Hamiltonians which can be efficiently studied by MCTDH calculations. It enables the description of more general Hamiltonians of the form

$$\begin{aligned} \hat{H} &= \sum_{t=1}^s V_t(x_1, x_2, \dots, x_{l_t}) \cdot \hat{H}_t, \\ \hat{H}_t &= \prod_{d=l_t+1}^f \hat{h}_t^{prim;d} \end{aligned} \quad (15)$$

which simultaneously include multi-dimensional functions  $V_t(x_1, x_2, \dots, x_i)$  and products of single-particle operators in the same term.<sup>4,78,101</sup> The matrix elements of these functions are computed using time-dependent quadratures based on grids obtained by diagonalizing the matrix representations of coordinate operators in the SPF bases.

Grid representations associated with the  $\phi_j^{\lambda|\lambda\circ\kappa}(x_a, x_b, \dots)$  are obtained by (approximate simultaneous) diagonalization of the coordinate matrices<sup>78,80</sup>

$$\langle \phi_j^{\lambda|\lambda\circ\kappa} | \hat{x}_n | \phi_i^{\lambda|\lambda\circ\kappa} \rangle, \quad n = a, b, \dots \quad (16)$$

The unitary matrix transforming to the (approximately) diagonal representation defines the basis-grid transformation  $\langle \xi_m^{\lambda|\lambda\circ\kappa} | \phi_i^{\lambda|\lambda\circ\kappa} \rangle$  and the grid points  $\xi_m^{\lambda|\lambda\circ\kappa}$  are given by

$$\langle \xi_n \rangle_m^{\lambda|\lambda\circ\kappa} = \langle \xi_m^{\lambda|\lambda\circ\kappa} | \hat{x}_n | \xi_m^{\lambda|\lambda\circ\kappa} \rangle, \quad n = a, b, \dots \quad (17)$$

Localized SPFs  $\xi_m^{\lambda|\lambda\circ\kappa}(x_a, x_b, \dots, t)$  associated with the grid points  $\xi_m^{\lambda|\lambda\circ\kappa}$  are defined by

$$|\xi_m^{\lambda|\lambda\circ\kappa}\rangle = \sum_j |\phi_j^{\lambda|\lambda\circ\kappa}\rangle \cdot \langle \phi_j^{\lambda|\lambda\circ\kappa} | \xi_m^{\lambda|\lambda\circ\kappa} \rangle. \quad (18)$$

Since the different coordinate matrices generally do not commute, only approximate simultaneous diagonalization is feasible for multi-dimensional  $\phi_j^{\lambda|\lambda\circ\kappa}$  and appropriate weighting and scaling of the coordinate matrices is important.<sup>81,98</sup>

The non-hierarchical CDVR approach employs operators  $\hat{V}_t^{CDVR}$  that include contributions from the grid representations associated with all nodes and edges to simulate the action of the potential  $V_t(x_1, x_2, \dots, x_{l_t})$  on a wavefunction.<sup>98,100</sup> The contribution from a node ( $\lambda$ ) is given by

$$\hat{V}_t^\lambda = \sum_N |\Xi_N^\lambda\rangle V_t(\Xi_N^\lambda) \langle \Xi_N^\lambda| \quad (19)$$

where

$$|\Xi_N^\lambda\rangle = \left| \prod_{\kappa=0}^\nu \xi_{j_\kappa}^{\lambda|\lambda\circ\kappa} \right\rangle \quad (20)$$

are grid-transformed configurations and

$$\Xi_N^\lambda = (\xi_{n_0}^{\lambda|\lambda\circ 0}, \xi_{n_1}^{\lambda|\lambda\circ 1}, \xi_{n_2}^{\lambda|\lambda\circ 1}, \dots) \quad (21)$$

defines a complete set of coordinate values. The contribution from an edge ( $\lambda \circ 0 | \lambda$ ),

$$\hat{V}_t^{\lambda \circ 0 | \lambda} = \hat{V}_t^{\lambda | \lambda \circ 0} = \sum_{n,m} |\Xi_{nm}^{\lambda \circ 0 | \lambda}\rangle V_t(\Xi_{n,m}^{\lambda \circ 0 | \lambda}) \langle \Xi_{nm}^{\lambda \circ 0 | \lambda}|, \quad (22)$$

is defined using grid-transformed edge-based configurations

$$|\Xi_{nm}^{\lambda \circ 0 | \lambda}\rangle = |\Xi_{mn}^{\lambda | \lambda \circ 0}\rangle = |\xi_n^{\lambda \circ 0 | \lambda}\rangle \cdot |\xi_m^{\lambda | \lambda \circ 0}\rangle \quad (23)$$

and the associated set of coordinates

$$\Xi_{n,m}^{\lambda \circ 0 | \lambda} = \Xi_{m,n}^{\lambda | \lambda \circ 0} = (\xi_n^{\lambda \circ 0 | \lambda}, \xi_m^{\lambda | \lambda \circ 0}). \quad (24)$$

The CDVR potential operator is given by

$$\hat{V}_t^{CDVR} = \sum_{\lambda \in \Lambda} \hat{V}_t^\lambda - \sum_{\substack{\lambda \in \Lambda \\ \lambda \neq \text{root}}} \hat{V}_t^{\lambda \circ 0 | \lambda} \quad (25)$$

where  $\Lambda$  denotes the set of all nodes.

To obtain the matrix elements  $\langle \Xi_I^\lambda | V_t | \Psi \rangle$ , the sum in Eq.(25) is rewritten separating contributions of the node  $\lambda$  and the  $\nu + 1$  subtrees originating from the  $\nu + 1$  edges connected to  $\lambda$ :

$$\hat{V}_t^{CDVR} = \hat{V}_t^\lambda + \sum_{\kappa=0}^\nu \Delta \hat{V}_t^{\lambda|\lambda\circ\kappa}. \quad (26)$$

The resulting expression reads<sup>99</sup>

$$\begin{aligned} \langle \Xi_I^\lambda | V_t | \Psi \rangle &= V_t(\Xi_I^\lambda) \cdot \langle \Xi_I^\lambda | \Psi \rangle \\ &\quad + \sum_\kappa \sum_l \langle \Xi_I^\lambda | \Xi_{l\kappa}^{\lambda|\lambda\circ\kappa} \rangle \\ &\quad \cdot \sum_{j_\kappa, k} \langle \Xi_{l\kappa}^{\lambda|\lambda\circ\kappa} | \Delta \hat{V}_t^{\lambda|\lambda\circ\kappa} | \Xi_{j_\kappa k}^{\lambda|\lambda\circ\kappa} \rangle \\ &\quad \cdot \sum_{J/J_\kappa} \langle \Xi_{j_\kappa k}^{\lambda|\lambda\circ\kappa} | \Xi_J^\lambda \rangle \cdot \langle \Xi_J^\lambda | \Psi \rangle. \end{aligned} \quad (27)$$

where  $J_{/κ}$  is short hand notation for  $(j_0, \dots, j_{κ-1}, j_{κ+1}, \dots)$ . All calculations required in the above equation can be implemented with a numerical effort scaling not worse than either  $n \cdot N$  or  $n^4$  where  $n$  denotes the number of SPFs associated with an edge and  $N$  the number of configurations associated with a node. Since  $N = n^d$  for a node with  $d$  edges and non-redundant nodes show at least three nodes, a  $n^4$  scaling is obtained for an optimally designed tree.

In Eq.(27), the matrix elements representing the edge-based contribution  $\Delta \hat{V}_t^{\lambda|\lambda\circ\kappa}$  to the potential operator in the basis of the edge-basis configurations  $\Xi_{nm}^{\lambda|\lambda\circ\kappa}$ ,

$$\Delta V_{t;iljk}^{\lambda|\lambda\circ\kappa} = \langle \Xi_{il}^{\lambda|\lambda\circ\kappa} | \Delta \hat{V}_t^{\lambda|\lambda\circ\kappa} | \Xi_{jk}^{\lambda|\lambda\circ\kappa} \rangle, \quad (28)$$

take a central role. They describes the CDVR correction to the potential operator  $\hat{V}_t^\lambda$  which only considers the grid  $\Xi_N^\lambda$  associated with the specific node. The recursive calculation of these matrix elements is particularly demanding. Introducing a modified potential operator

$$\hat{V}_{t,\kappa}^\lambda = \hat{V}_t^\lambda + \sum_{\substack{\mu \\ \mu \neq \kappa}} \Delta \hat{V}_t^{\lambda|\lambda\circ\mu} \quad (29)$$

where a single correction term  $\hat{V}_t^{\lambda|\lambda\circ\kappa}$  is omitted in  $\hat{V}_t$ , these matrix element can be computed by<sup>99</sup>

$$\begin{aligned} \Delta V_{t;nlmk}^{\lambda\circ\kappa|\lambda} &= -V_t(\Xi_{n,l}^{\lambda\circ\kappa|\lambda}) \cdot \delta_{nm} \cdot \delta_{lk} \\ &+ \sum_I \langle \Xi_{nl}^{\lambda\circ\kappa|\lambda} | \Xi_I^\lambda \rangle \cdot \langle \Xi_I^\lambda | \hat{V}_{t,\kappa}^\lambda | \Xi_{mk}^{\lambda\circ\kappa|\lambda} \rangle. \end{aligned} \quad (30)$$

Here for any index pair  $m, k$  the matrix element  $\langle \Xi_I^\lambda | \hat{V}_{t,\kappa}^\lambda | \Xi_{m,k}^{\lambda\circ\kappa|\lambda} \rangle$  can be calculated analogously to the matrix element  $\langle \Xi_I^\lambda | V_t | \Psi \rangle$  on the left hand side of Eq.(27). Thus, the numerical effort required for the calculation of the  $\Delta \hat{V}_{t;iknm}^{\lambda\circ\kappa|\lambda}$  scales as  $n^2$  times (where  $n$  denotes the number of SPFs associated with an edge) the numerical effort required for the evaluation of Eq.(27), resulting a  $n^6$  scaling for an optimally designed tree.

This  $n^6$  scaling can be viewed as one important disadvantage of the CDVR approach: conventional MCTDH calculations relying on a SOP form of the Hamiltonian achieve a  $n^4$  scaling for optimally designed trees. Another disadvantage of the non-hierarchical CDVR scheme described above is the appearance of the node-edge transformation, described by the matrices  $\langle \Xi_{j\kappa k}^{\lambda|\lambda\circ\kappa} | \Xi_j^\lambda \rangle$ , in Eq.(27). This transformation affects all coordinates of the system. Consequently, the CDVR-potential operator effectively acts not only the  $l$  coordinates present in  $V_t(x_1, x_2, \dots, x_l)$  but on all coordinates of the system. This undesirable effect and different schemes to mitigate the consequences have been discussed in detail in Ref.99. Both shortcomings will be addressed by the revised CDVR scheme described in the following.

#### IV. A REVISED NON-HIERARCHICAL CDVR

The issues discussed above can be addressed by replacing the edge-based contribution to the potential operator appearing in Eq.(27),

$$\Delta \hat{V}_t^{\lambda|\lambda\circ\kappa} = \sum_{i,l,j,k} |\Xi_{jk}^{\lambda|\lambda\circ\kappa}\rangle \cdot \Delta V_{t;iljk}^{\lambda|\lambda\circ\kappa} \cdot \langle \Xi_{il}^{\lambda|\lambda\circ\kappa}|, \quad (31)$$

by the revised operator

$$\Delta \hat{V}_{t,rev}^{\lambda|\lambda\circ\kappa} = \sum_{i,j} |\xi_i^{\lambda|\lambda\circ\kappa}\rangle \cdot \Delta V_{t;ij}^{\lambda|\lambda\circ\kappa} \cdot \langle \xi_j^{\lambda|\lambda\circ\kappa}|. \quad (32)$$

The revised operator no longer refers to the transformed SHFs  $\xi_i^{\lambda\circ\kappa|\lambda}$  and thus avoids projection onto the space spanned by the SHF. Consequently, the revised operator of Eq.(32) acts for  $\kappa > 0$  only on the  $l$  coordinates present in  $V_t(x_1, x_2, \dots, x_l)$  and does not affect any other coordinates.

The revised operator is chosen to optimally approximate the original operator  $\Delta \hat{V}_t^{\lambda|\lambda\circ\kappa}$  in

$$V_t(x_1, x_2, \dots, x_{l_t}) \cdot \hat{H}_t | \Psi \rangle. \quad (33)$$

It is obtained by minimizing

$$\left\| \left( \Delta \hat{V}_t^{\lambda|\lambda\circ\kappa} - \Delta \hat{V}_{t,rev}^{\lambda|\lambda\circ\kappa} \right) \hat{H}_t | \Psi \right\|^2 \quad (34)$$

with respect to the  $\Delta \hat{V}_{t;ij}^{\lambda|\lambda\circ\kappa}$ . As described in detail in Appendix A, the variation yields

$$\begin{aligned} \Delta V_{t;ij}^{\lambda|\lambda\circ\kappa} &= \sum_n u_{t;jn}^{\lambda|\lambda\circ\kappa} \sum_m u_{t;im}^{\lambda|\lambda\circ\kappa*} \cdot \frac{1}{r_{t;n}^{\lambda|\lambda\circ\kappa} + r_{t;m}^{\lambda|\lambda\circ\kappa}} \\ &\cdot \sum_l u_{t;ln}^{\lambda|\lambda\circ\kappa*} \sum_k u_{t;km}^{\lambda|\lambda\circ\kappa} \left( X_{t;kl}^{\lambda|\lambda\circ\kappa*} + X_{t;lk}^{\lambda|\lambda\circ\kappa} \right) \end{aligned} \quad (35)$$

with

$$X_{t;lk}^{\lambda|\lambda\circ\kappa} = \sum_i \langle \hat{H}_t | \Psi | \Xi_{li}^{\lambda|\lambda\circ\kappa} \rangle \sum_{j,n} \Delta \hat{V}_{t;kinj}^{\lambda|\lambda\circ\kappa} \langle \Xi_{nj}^{\lambda|\lambda\circ\kappa} | \hat{H}_t | \Psi \rangle. \quad (36)$$

The  $r_{t;n}^{\lambda|\lambda\circ\kappa}$  and  $u_{t;in}^{\lambda|\lambda\circ\kappa}$  in the Eq.(35) are eigenvalues and eigenvectors defined by the eigenvalue problem

$$\langle \hat{H}_t | \Psi | \xi_i^{\lambda|\lambda\circ\kappa} \rangle \langle \xi_j^{\lambda|\lambda\circ\kappa} | \hat{H}_t | \Psi \rangle = \sum_n u_{t;in}^{\lambda|\lambda\circ\kappa} \cdot r_{t;n}^{\lambda|\lambda\circ\kappa} \cdot u_{t;jn}^{\lambda|\lambda\circ\kappa*}. \quad (37)$$

Replacing  $\Delta \hat{V}_t^{\lambda|\lambda\circ\kappa}$  by  $\Delta \hat{V}_{t,rev}^{\lambda|\lambda\circ\kappa}$  in Eq.(27), the action of a term  $V_t \cdot \hat{H}_t$  in the Hamiltonian (15) on the wavefunction at node ( $\lambda$ ) can be evaluated by

$$\begin{aligned} \langle \Xi_I^\lambda | \hat{V}_t | \hat{H}_t | \Psi \rangle &= V_t(\Xi_I^\lambda) \cdot \langle \Xi_I^\lambda | \hat{H}_t | \Psi \rangle \\ &+ \sum_{\kappa} \sum_{j\kappa} \Delta V_{t;i\kappa j\kappa}^{\lambda|\lambda\circ\kappa} \cdot \langle \Xi_{I/j\kappa}^\lambda | \hat{H}_t | \Psi \rangle \end{aligned} \quad (38)$$

where  $(I_{/\kappa}, j_\kappa)$  is short hand notation for  $(i_0, \dots, i_{\kappa-1}, j_\kappa, i_{\kappa+1}, \dots)$ . In contrast to Eq.(27), this equation no longer includes any projection onto spaces spanned by the edge-based configurations  $\Xi_{nm}^{\lambda|\lambda\circ\kappa}$ .

The CDVR corrections appear in Eq.(38) in form of the matrices  $\Delta \hat{V}_t^{\lambda|\lambda\circ\kappa}$ . These can be straightforwardly computed via Eq.(35) once the matrices  $\mathbf{X}_t^{\lambda|\lambda\circ\kappa}$  defined in Eq.(36) are known. The required  $\mathbf{X}_t^{\lambda\circ\kappa|\lambda}$  (the change in the superscripts is required for notational reasons),

$$X_{t;lk}^{\lambda\circ\kappa|\lambda} = \sum_i \langle \hat{H}_t \Psi | \Xi_{li}^{\lambda\circ\kappa|\lambda} \rangle \sum_{j,n} \Delta \hat{V}_{t;kinj}^{\lambda\circ\kappa|\lambda} \langle \Xi_{nj}^{\lambda\circ\kappa|\lambda} | \hat{H}_t \Psi \rangle, \quad (39)$$

are obtained by inserting Eq.(30) into Eq.(39):

$$\begin{aligned} X_{t;lk}^{\lambda\circ\kappa|\lambda} &= - \sum_i \langle \hat{H}_t \Psi | \Xi_{li}^{\lambda\circ\kappa|\lambda} \rangle V_t(\Xi_{k,i}^{\lambda\circ\kappa|\lambda}) \langle \Xi_{ki}^{\lambda\circ\kappa|\lambda} | \hat{H}_t \Psi \rangle \\ &\quad + \sum_i \langle \hat{H}_t \Psi | \Xi_{li}^{\lambda\circ\kappa|\lambda} \rangle \sum_{j,n} \sum_I \langle \Xi_{ki}^{\lambda\circ\kappa|\lambda} | \Xi_I^\lambda \rangle \\ &\quad \cdot \langle \Xi_I^\lambda | \hat{V}_{t,\kappa}^\lambda | \Xi_{nj}^{\lambda\circ\kappa|\lambda} \rangle \langle \Xi_{nj}^{\lambda\circ\kappa|\lambda} | \hat{H}_t \Psi \rangle \\ &= - \sum_i \langle \hat{H}_t \Psi | \Xi_{li}^{\lambda\circ\kappa|\lambda} \rangle V_t(\Xi_{k,i}^{\lambda\circ\kappa|\lambda}) \langle \Xi_{ki}^{\lambda\circ\kappa|\lambda} | \hat{H}_t \Psi \rangle \\ &\quad + \sum_i \langle \hat{H}_t \Psi | \Xi_{li}^{\lambda\circ\kappa|\lambda} \rangle \sum_{I_{/\kappa}} \langle \Xi_{ki}^{\lambda\circ\kappa|\lambda} | \Xi_{I_{/\kappa}i}^\lambda \rangle \\ &\quad \cdot \langle \Xi_{I_{/\kappa}i}^\lambda | \hat{V}_{t,\kappa}^\lambda \left( \sum_{n,j} |\Xi_{nj}^{\lambda\circ\kappa|\lambda} \rangle \langle \Xi_{nj}^{\lambda\circ\kappa|\lambda} | \hat{H}_t \Psi \right) \rangle. \end{aligned} \quad (40)$$

In contrast to Eq.(30), here  $\hat{V}_{t,\kappa}^\lambda$  acts only on a single wavefunction  $\tilde{\Psi}$  given by

$$\tilde{\Psi} = \sum_{n,j} |\Xi_{nj}^{\lambda\circ\kappa|\lambda} \rangle \langle \Xi_{nj}^{\lambda\circ\kappa|\lambda} | \hat{H}_t \Psi. \quad (41)$$

The action of  $\hat{V}_{t,\kappa}^\lambda$  on  $\tilde{\Psi}$  at the node  $(\lambda)$  can be computed using a scheme analogous to Eq.(38) with a numerical effort scaling as  $n \cdot N$  where  $n$  denotes the number of SPFs associated with an edge and  $N$  the number of configurations associated with a node. Consequently, the numerical effort associated with the computation of the  $\mathbf{X}_t^{\lambda\circ\kappa|\lambda}$  and the  $\hat{V}_{t;ij}^{\lambda\circ\kappa|\lambda}$  also scales as  $n \cdot N$ . For an ideally structured tree, the revised non-hierarchical CDVR can thus be implemented with no part of the calculation scaling worse than  $n^4$ .

The revised CDVR described above yields accurate results for separable potentials (see Appendix B for a derivation). Thus, the optimal separable potentials discussed in the context of the original non-hierarchical CDVR in Ref.99 become obsolete in the revised CDVR.

## V. QUADRATURE OPTIMIZED SPFS

Unoccupied SPFs do not contribute to the wavefunction representation and can thus be redefined to increase

the accuracy of the CDVR quadrature. A scheme to define artificial SPFs that systematically increase the accuracy of the CDVR quadrature has been introduced in Ref.100. A set of additional SPFs at the edge  $(\lambda \circ \kappa | \lambda)$  can be obtained by diagonalizing the operator

$$\hat{A}^{\lambda\circ\kappa|\lambda} = (1 - \hat{P}^{\lambda\circ\kappa|\lambda}) \left( \sum_i \hat{x}_i \hat{\rho}^{\lambda\circ\kappa|\lambda} \hat{x}_i \right) (1 - \hat{P}^{\lambda\circ\kappa|\lambda}) \quad (42)$$

where the index  $i$  numbers all physical coordinates  $x_i$  present  $\phi^{\lambda\circ\kappa|\lambda}$  and

$$\hat{\rho}^{\lambda\circ\kappa|\lambda} = \sum_{j,l} |\phi_l^{\lambda\circ\kappa|\lambda} \rangle \rho_{jl}^{\lambda\circ\kappa|\lambda} \langle \phi_j^{\lambda\circ\kappa|\lambda} |, \quad (43)$$

$$\hat{P}^{\lambda\circ\kappa|\lambda} = \sum_m |\phi_m^{\lambda\circ\kappa|\lambda} \rangle \langle \phi_m^{\lambda\circ\kappa|\lambda} |. \quad (44)$$

The eigenstates corresponding to largest eigenvalues of  $\hat{A}^{\lambda\circ\kappa|\lambda}$  define artificial SPFs that should be added to the SPF basis to improve the accuracy of the CDVR quadrature. If the number of artificial SPFs resulting from  $\hat{A}^{\lambda\circ\kappa|\lambda}$  is not sufficient, similar operators including higher powers of the  $x_i$  can be devised<sup>100</sup>. For simplicity, these extensions will not be considered here explicitly.

Experience resulting from various test calculations showed that the use of additional SPFs following this schemes negatively affects the time steps used by the constant mean field (CMF) scheme<sup>102,103</sup> employed to integrate the MCTDH equations of motion. The artificial SPFs tend to varying strongly with time forcing the integrator to update the matrix elements extremely frequently. To address this issue, the modified scheme described below has been devised.

In the modified scheme, the operator

$$\hat{B}^{\lambda\circ\kappa|\lambda} = \hat{\rho}^{\lambda\circ\kappa|\lambda} + \epsilon_{unocc} \cdot \left( \sum_i \hat{x}_i \hat{\rho}^{\lambda\circ\kappa|\lambda} \hat{x}_i \right) \quad (45)$$

is diagonalized. Here  $\epsilon_{unocc}$  defines the threshold value when a SPF is considered unoccupied. If  $n$  SPFs are employed and all  $n$  eigenvalues of  $\hat{\rho}^{\lambda\circ\kappa|\lambda}$  are significantly larger than  $\epsilon_{unocc}$ , the space spanned by the  $n$  largest eigenvalues of  $\hat{B}^{\lambda\circ\kappa|\lambda}$  is identical to the space spanned by the  $n$  original SPFs. However, if  $m$  SPFs show populations significantly smaller than  $\epsilon_{unocc}$  and  $(n - m)$  SPFs show populations significantly larger than  $\epsilon_{unocc}$ , the space spanned by the  $n$  largest eigenvalues of  $\hat{B}^{\lambda\circ\kappa|\lambda}$  consists of the  $(n - m)$  populated SPFs and  $m$  artificial SPFs similar to the eigenvectors corresponding to the  $m$  largest eigenvalues of  $\hat{A}^{\lambda\circ\kappa|\lambda}$ . In intermediate situations, eigenstates of  $\hat{B}^{\lambda\circ\kappa|\lambda}$  appear that are mixtures of SPFs with populations close to  $\epsilon_{unocc}$  and relevant eigenstates of  $\hat{A}^{\lambda\circ\kappa|\lambda}$ .

The eigenstates  $|b_i^{\lambda,\kappa}\rangle$  corresponding to the  $n$  largest eigenvalues  $b_i^{\lambda,\kappa}$  of  $\hat{B}^{\lambda\circ\kappa|\lambda}$  are then used to obtain an improved set of  $n$  new SPFs  $\phi_i^{\lambda\circ\kappa|\lambda}$ . Specifically, first a

set of  $n$  orthonormal functions

$$|\chi_i^{\lambda,\kappa}\rangle = \sum_{j=1}^n U_{i,j}^{\lambda,\kappa} |b_j^{\lambda,\kappa}\rangle \quad (46)$$

is constructed where the unitary transformation matrix  $U^{\lambda,\kappa}$  is chosen to maximize the overlap between the old SPFs  $\phi_i^{\lambda\circ\kappa|\lambda}$  and the new  $\chi_i^{\lambda,\kappa}$ . Assigning a population  $b_i^{\lambda,\kappa}$  to each state  $|b_i^{\lambda,\kappa}\rangle$ , the corresponding wavefunction reads (see Eq.(7))

$$|\Psi^{\lambda,\kappa}\rangle = \sum_{i,j} U_{i,j}^{\lambda,\kappa} \left(b_j^{\lambda,\kappa}\right)^{\frac{1}{2}} |b_j^{\lambda,\kappa} \phi_i^{\lambda|\lambda\circ\kappa}\rangle. \quad (47)$$

Here the superscript  $\lambda, \kappa$  indicates that the new wavefunction is constructed using a new set of SPFs associated with the edge  $(\lambda \circ \kappa | \lambda)$ .

The coefficients  $\tilde{A}_I^\lambda$  of Eq.(10) enter in the definition of all  $\phi_i^{\lambda\circ\kappa|\lambda}$  associated with any edge connected to the node  $(\lambda)$ . However, different revised wavefunctions  $|\Psi^{\lambda,\kappa}\rangle$  result from Eq.(47) for different choices of  $\kappa$ . To equally account for the effects of all edges, the new  $\tilde{A}_I^\lambda$  are computed using the average of all  $|\Psi^{\lambda,\kappa}\rangle$ :

$$\tilde{A}_I^\lambda = \langle \Phi_I^\lambda | \Psi \rangle = \frac{1}{\nu + 1} \sum_{\kappa=0}^{\nu} \langle \Phi_I^\lambda | \Psi^{\lambda,\kappa} \rangle. \quad (48)$$

Finally, the new  $A_{i_0, i_1, \dots, i_\nu}^\lambda$  are obtained from the new  $\tilde{A}_{i_0, i_1, \dots, i_\nu}^\lambda$  by symmetric reorthogonalization with respect to the index  $i_0$ .

As a result of replacing the  $\tilde{A}_I^\lambda$  at all nodes  $(\lambda)$  accordingly, a revised wavefunction is obtained where SPFs showing tiny populations are replaced by artificial SPFs improving the quadrature accuracy. Since these artificial SPFs show populations of the order of  $\epsilon_{unocc}$ , the revised wavefunction slightly differs from the original one. Thus,  $\epsilon_{unocc}$  has to be chosen sufficiently small to assure that relevant observables are not affected by these populations. However, assigning these small populations to the artificial SPFs guarantees their short time stability during the propagation and successfully addresses the aforementioned problem with the short integration steps. In all calculations employing this scheme presented in Sect.VI.C, time steps comparable to the ones required in analogous standard MCTDH calculations have been observed.

## VI. NUMERICAL EXAMPLES

The properties of the revised non-hierarchical CDVR are illustrated studying typical examples already considered in previous work on the CDVR approach<sup>4,78,80,81,98–100</sup>: the photodissociation of NOCl, the vibrational states of the methyl radical, and the  $S_0 \rightarrow S_2$  excitation in pyrazine.

### A. Photodissociation of NOCl

The description of the photodissociation of NOCl closely follows Ref. 2. A  $NO + Cl$  Jacobi construction and the Jacobi coordinates  $r, R$  and  $\theta$  are used. The PES is derived from an ab initio potential developed by Schinke et al.<sup>104</sup> and refitted to the form<sup>2</sup>

$$V(r, R, \theta) = \sum_i c_i \cdot v_i^{(R)}(R) \cdot v_i^{(r)}(r) \cdot v_i^{(\theta)}(\theta). \quad (49)$$

The initial wavefunction is a Gaussian wave packet modeling the vibrational ground state of the  $S_0$  potential energy surface. Due to the SOP form of the PES, potential matrix elements can efficiently be calculated either with or without the CDVR approach. The same number of SPFs,  $n$ , is used in all degrees of freedom.

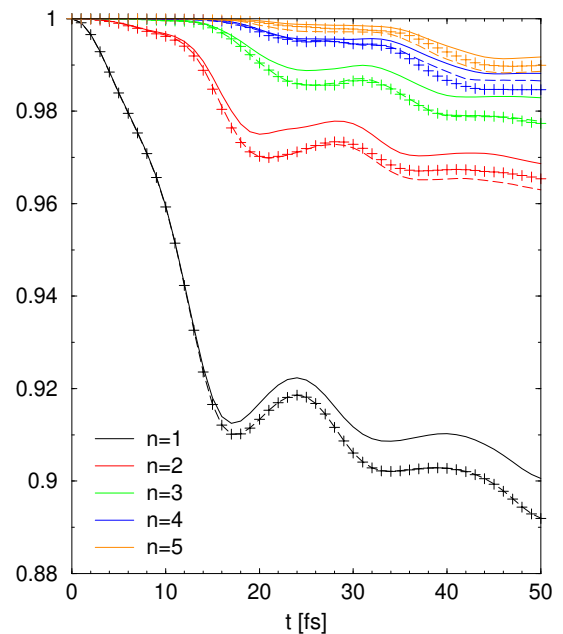


FIG. 2: Photodissociation of NOCl: real part of the overlap of a MCTDH wavefunction and the numerically exact reference wavefunction. Results of different types of MCTDH calculations are shown using different line styles: solid lines for calculations using exact potential energy matrix elements, dashed lines for calculations using the original non-hierarchical CDVR of Refs.98,99, and plus signs for calculations using the revised non-hierarchical CDVR. MCTDH calculations with different SPF numbers  $n$  are displayed using different colors as indicated in the legend.

In Fig.2, the accuracy of MCTDH calculations using revised non-hierarchical CDVR approach is compared to the accuracy achieved in MCTDH calculations using a SOP representation of the potential or the original non-hierarchical CDVR<sup>98,99</sup>. Specifically, the real part of the overlap of a MCTDH wavefunction and the numerically exact reference wavefunction is given. The real part of the overlap directly measures the accuracy of the propagated MCTDH wavefunction since

$\|\psi_1 - \psi_2\|^2 = 2[1 - \text{Re}(\langle \psi_1 | \psi_2 \rangle)]$ . Different SPF basis set sizes ranging from Hartree level,  $n = 1$ , to effectively converged basis set sizes,  $n = 5$ , are considered.

Differences between the accuracy obtained with the original and the revised CDVR scheme are minor. Depending on the number of SPFs employed, the results computed with the revised scheme can be either slightly more or slightly less accurate than the ones obtained with the original non-hierarchical CDVR. In general, the inaccuracies resulting from the use of either CDVR scheme are significantly smaller than errors caused by the limited size of the SPF basis.

### B. Vibrational states of methyl

The description of the methyl radical,  $\text{CH}_3$ , closely follows Ref.105. The coordinate system and quasi-exact kinetic energy operator developed in Ref.106 and the potential energy surface of Medvedev et al.<sup>107</sup> are used. The coordinates  $\rho$  and  $\vartheta, \varphi$  describe the totally symmetric and e-symmetric stretching modes, respectively. The umbrella bending and e-symmetric bending motions are described by the coordinates  $\theta$  and coordinates  $\phi, \chi$ , respectively. Block relaxation within the state-averaged MCTDH approach<sup>105</sup> is used to compute the vibrational eigenstates. The calculations employ the DVR schemes and number of grid points as described in Ref. 105. The number of SPFs employed in the coordinates  $\rho, \theta, \vartheta, \varphi, \phi$ , and  $\chi$  is 4, 8, 8, 4, 6, and 6, respectively.

Tab. I lists the first 36 vibrational levels computed with MCTDH calculations employing the revised non-hierarchical CDVR introduced in the present work. The computed energies are compared to results of the original non-hierarchical CDVR taken from Ref.98 and accurate reference results taken from Ref.106. As already seen in the previous example studied in Sect.VIA, the accuracy achieved with the revised CDVR scheme is roughly equal to the accuracy of the original non-hierarchical CDVR. On average, the results computed with the revised scheme appear to be slightly more accurate than the ones reported for the original scheme in Ref.98. However, given the numerical uncertainties resulting from the choice of the various accuracy and regularization parameters employed in the different calculations, these differences should not be considered significant.

### C. The $S_0 \rightarrow S_2$ excitation in pyrazine

The  $S_0 \rightarrow S_2$  excitation in pyrazine is benchmark example of non-adiabatic dynamics on conically intersecting PESs.<sup>58–60,108–116</sup> The dynamics following the  $S_0 \rightarrow S_2$  excitation proceeds in steps (see, e.g., Ref.112 for a detailed discussion): a compact wavepacket starts its motion on the upper ( $S_2$ ) adiabatic potential energy surface (PES), reaches the conical intersection between the  $S_2$  and  $S_1$  surfaces, and undergoes an essentially com-

TABLE I: Zero point energy and vibrational excitation energies  $E_{\nu_1\nu_2\nu_3\nu_4}$  of  $\text{CH}_3$  (in  $\text{cm}^{-1}$ ;  $\nu_1, \nu_2, \nu_3$ , and  $\nu_4$  label excitations in the totally symmetric stretching, e-symmetric stretching, umbrella bending, and e-symmetric bending modes, respectively). Results of MCTDH calculations using the revised CDVR approach are compared with results of original non-hierarchical CDVR<sup>98</sup> and numerically exact results<sup>106</sup>. Differences  $\Delta E_{\nu_1\nu_2\nu_3\nu_4}$  between the MCTDH results and the results of Ref. 106 indicate the error resulting from the CDVR quadrature.

$(\nu_1\nu_2\nu_3\nu_4)$	Ref.106	Ref.98 (CDVR)		revised CDVR	
	E	E	$\Delta E$	E	$\Delta E$
(0000)	6445.2	6445.1	0.1	6445.2	0
(0100)	591.5	591.4	0.1	591.4	0.1
(0200)	1265.7	1265.6	0.1	1265.7	0
(0001)	1388.2	1388.2	0	1388.2	0
	1388.5	1388.4	0.1	1388.5	0
(0101 <sup>1</sup> )	1991.4	1991.3	0.1	1991.3	0.1
	1991.9	1991.9	0	1991.9	0
(0300)	1993.4	1993.3	0.1	1993.3	0.1
(0201 <sup>1</sup> )	2673.2	2673.2	0	2673.2	0
	2673.3	2674.1	0.8	2674.1	0.8
(0002 <sup>0</sup> )	2750.7	2750.6	0.1	2750.7	0
(0400)	2762.3	2762.2	0.1	2762.3	0
(0002 <sup>2</sup> )	2767.6	2767.5	0.1	2767.6	0
	2767.6	2767.6	0	2767.6	0
(1000)	2989.7	2989.0	0.7	2989.7	0
(001 <sup>1</sup> 0)	3142.3	3143.3	0.9	3141.8	0.5
	3142.6	3143.9	1.3	3142.6	0
(0102 <sup>0</sup> )	3367.3	3367.2	0.1	3367.2	0.1
(0102 <sup>2</sup> )	3382.7	3382.6	0.1	3382.7	0
	3382.8	3382.8	0	3382.8	0
(0301 <sup>1</sup> )	3406.6	3406.5	0.1	3406.5	0.1
	3407.9	3407.7	0.2	3407.8	0.1
(0500)	3556.8	3556.0	0.8	3555.5	1.3
(1100)	3573.1	3572.0	1.1	3572.4	0.7
(011 <sup>1</sup> 0)	3709.3	3710.4	1.1	3708.8	0.5
	3709.6	3711.0	1.4	3709.7	0.1
(0202 <sup>0</sup> )	4057.8	4057.6	0.2	4057.6	0.2
(0202 <sup>2</sup> )	4072.7	4072.6	0.1	4072.6	0.1
	4073.0	4072.9	0.1	4072.9	0.1
(0003 <sup>1</sup> )	4107.8	4107.6	0.2	4107.1	0.7
	4108.5	4108.6	0.1	4108.0	0.5
(0003 <sup>3</sup> )	4137.5	4137.5	0	4137.6	0.1
(0003 <sup>3</sup> )	4138.3	4138.2	0.1	4138.0	0.3
(0401 <sup>1</sup> )	4178.3	4178.4	0.1	4178.3	0
	4179.9	4180.7	0.8	4179.9	0
(1200)	4234.7	4233.2	1.5	4233.6	1.1
mean $\Delta E$			0.4		0.2

plete transition into the lower adiabatic ( $S_1$ ) electronic state. In the subsequent motion on the lower adiabatic PES, the wavepacket rapidly fragments and visits almost the entire accessible phase space. The description of the different steps, which show very different dynamical character, provides a challenging test for any quantum dynamics method.

The full-dimensional (24D) quantum dynamic calculations employ the coupled diabatic PESs developed by Raab et al.<sup>60</sup> The Hamiltonian reads

$$\hat{H} = \sum_{n=1}^{24} \frac{\omega_n}{2} \left( -\frac{\partial^2}{\partial q_n^2} + q_n^2 \right) + \begin{pmatrix} V_1(\mathbf{q}) & V_c(\mathbf{q}) \\ V_c(\mathbf{q}) & V_2(\mathbf{q}) \end{pmatrix} \quad (50)$$

with

$$V_i(\mathbf{q}) = \sum_{n=1}^{24} a_n^{(i)} q_n + \sum_{n=1}^{24} \sum_{m=n+1}^{24} b_{n,m}^{(i)} q_n q_m \quad (51)$$

(many of the  $a_n^{(i)}$  and  $b_{n,m}^{(i)}$  parameters vanish due to symmetry). It shows a sum of products (SOP) form and thus can be readily be used in MCTDH calculations without requiring CDVR.

The description used in the present work closely follows Ref.99 where the quantum dynamics in  $S_0 \rightarrow S_2$  excited pyrazine was used to study the accuracy of the non-hierarchical CDVR. The same tree structure and time-independent basis sets are used in the MCTDH wavefunction representation. As in Ref.99, the Hamiltonian is written as

$$\hat{H} = \sum_{n=1}^{24} \frac{\omega_n}{2} \left( -\frac{\partial^2}{\partial q_n^2} + q_n^2 \right) + V_1(\mathbf{q}) \cdot \begin{pmatrix} 1 & 0 \\ 0 & 0 \end{pmatrix} + V_2(\mathbf{q}) \cdot \begin{pmatrix} 0 & 0 \\ 0 & 1 \end{pmatrix} + V_c(\mathbf{q}) \cdot \begin{pmatrix} 0 & 1 \\ 1 & 0 \end{pmatrix} \quad (52)$$

to obtain the form specified in Eq.(15) for CDVR calculations. Beside the SPF basis set used in Ref.99, additional larger basis set are considered. The use of larger basis sets in MCTDH/CDVR calculations is facilitated by the increased numerical efficiency of the revised CDVR scheme introduced in Sect.IV. All SPF basis set employed are specified in Tab.II.

Basis set B0 to B4 have already been used in Ref.99. The new basis set B5 was obtained by increasing the number of all SPFs by about 15 percent compared to basis B4. This increases the total number of A-coefficients and CDVR grid points by a factor of about 1.5 compared to basis set B4. An even larger basis R was designed to provide reference wavefunctions of comparatively high accuracy.

In Figs. 3 to 5, results obtained by MCTDH calculations using different non-hierarchical CDVR schemes are compared to the results of MCTDH calculations employing exact potential energy matrix elements (i.e., MCTDH calculation using a SOP representation of the entire Hamiltonian). In each figure, the results of MCTDH

TABLE II: Number of SPFs employed at each edge in the different MCTDH calculations (for the definition of the tree used in the wavefunction representation see Ref.99).

edge	SPFs in basis						
	B0	B1	B2	B3	B4	B5	R
1;1	10	20	32	41	49	57	80
2;11	11	13	15	18	22	26	50
2;12	5	6	7	11	13	15	40
1;2	6	7	10	13	16	19	40
2;21	4	6	6	8	10	12	40
3;211	4	5	4	6	7	8	18
3;212	3	3	3	4	5	6	10
2;22	4	4	5	6	7	8	20
1;3	9	17	28	36	43	49	80
2;31	5	6	15	19	23	27	50
3;311	3	5	7	11	13	15	50
4;3111	3	5	7	9	11	13	50
5;31111	2	4	4	5	6	7	12
5;31112	3	3	4	5	6	7	24
4;3112	2	2	2	3	4	5	6
3;312	4	9	14	20	24	28	50
4;3121	3	6	9	12	14	16	50
5;31211	3	5	7	9	11	13	50
6;312111	2	4	5	4	5	6	20
6;312112	3	3	4	4	5	6	16
5;31212	3	3	4	4	5	6	8
4;3122	3	5	8	11	13	15	50
5;31221	3	4	6	7	8	9	50
6;312211	3	4	4	6	7	8	20
6;312212	2	2	3	3	4	5	7
5;31222	3	4	4	5	6	7	16
2;32	8	14	26	33	40	47	80
3;321	7	13	20	15	18	21	50
4;3211	4	11	17	20	24	28	50
4;3212	5	12	19	23	28	33	50
3;322	6	14	24	31	37	43	80
4;3221	5	7	11	11	13	15	50
5;32211	5	7	9	11	13	15	50
6;322111	2	2	3	4	5	6	8
6;322112	5	7	8	10	12	14	32
5;32212	2	3	4	8	10	12	50
6;322121	2	2	3	3	4	5	8
6;322122	2	3	4	4	5	6	10
4;3222	4	8	11	14	17	20	50
5;32221	2	3	3	4	5	6	42
6;322211	2	2	3	3	4	5	6
6;322212	2	3	3	4	5	6	8
5;32222	5	7	9	10	12	14	50
6;322221	3	4	5	6	7	8	40
6;322222	4	5	5	6	7	8	12
1;4	2	2	2	2	2	2	2

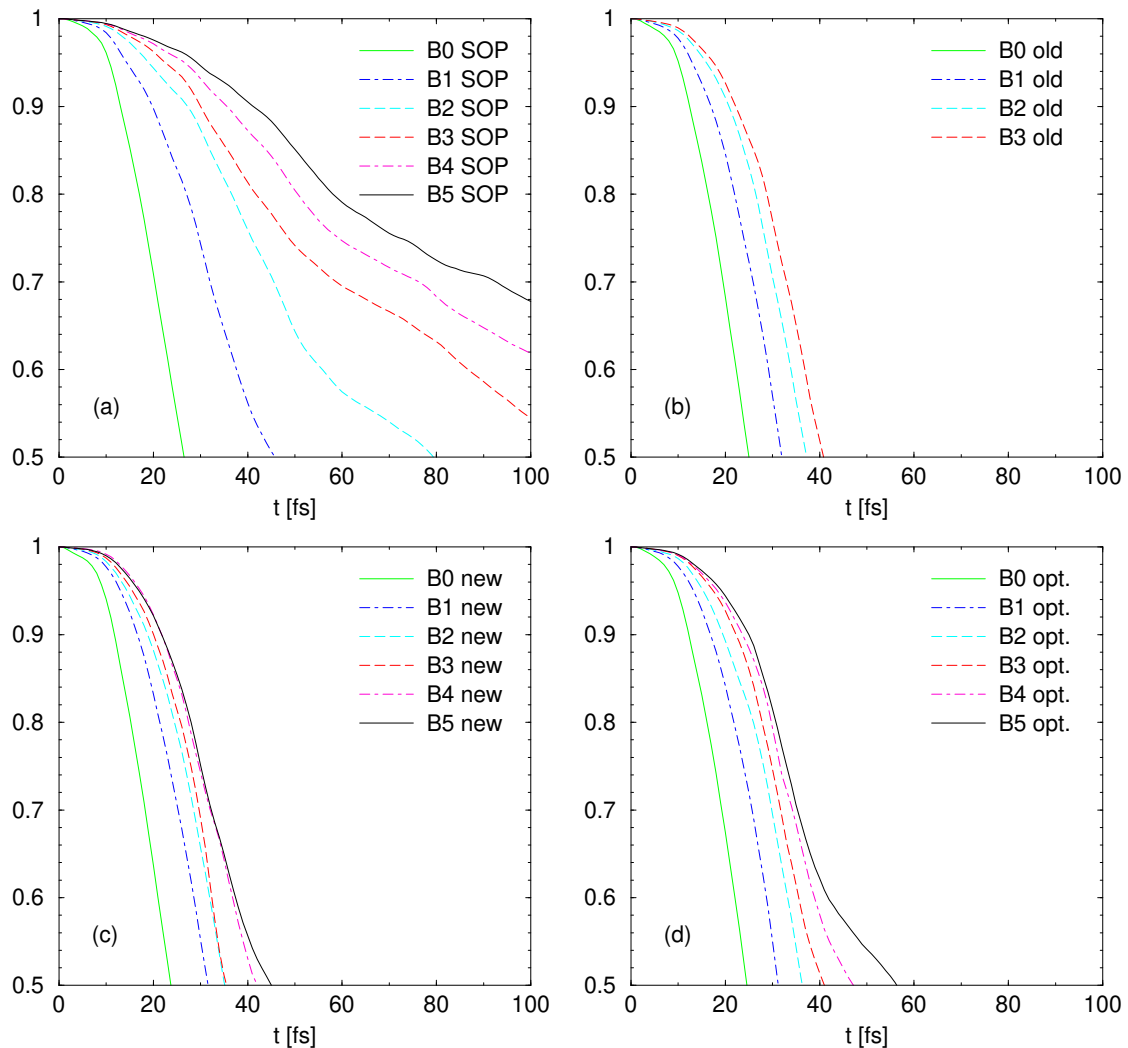


FIG. 3: Real part of the overlap  $\langle \psi_{B6,SOP}(t) | \psi(t) \rangle$  between the MCTDH wavefunctions  $\psi(t)$  obtained by different calculations with reference results obtained with the basis R and a SOP representation of the Hamiltonian: Panels (a) to (d) show results of MCTDH calculations using a SOP representation, the original non-hierarchical CDVR approach<sup>99</sup>, the revised non-hierarchical CDVR approach of the present work, and the revised non-hierarchical CDVR approach with optimized unoccupied SPFs (see text for details), respectively. Results obtained with different SPF basis sets size as indicated in the legend are displayed.

calculations using the SOP representation are shown in panel (a) and the results computed with original non-hierarchical CDVR taken from Refs.99 are displayed in panel (b). Panel (c) shows results obtained with revised non-hierarchical CDVR approach introduced in the present work. Results using the revised non-hierarchical CDVR approach and the quadrature optimized SPFs described in Sect.V are displayed in panel (d). In the calculations with the quadrature optimized SPFs, a threshold value of  $\epsilon_{unocc} = 10^{-8}$  has been used.

In Fig.3, the accuracy of MCTDH wavefunctions computed using different schemes and SPF basis set sizes is compared. The real part of the overlap of a MCTDH wavefunction and the reference wavefunction computed employing the reference basis R and the SOP representation of the Hamiltonian are shown. Since

$\|\psi - \psi_{R,SOP}\|^2 = 2[1 - \text{Re}(\langle \psi_{R,SOP} | \psi \rangle)]$ , the real part of the overlap directly measures the accuracy the propagated MCTDH wavefunction.

As already discussed in the previous work on the original non-hierarchical CDVR, the relative accuracy achieved with the SOP and CDVR approaches vary strongly depending on the size of the SPF basis. For the small B0 basis, the differences between the SOP and any of the CDVR results are minor. Here the additional error introduced by the CDVR quadrature is small compared to the error in the wavefunction representation resulting for the small SPF basis. Considering larger SPF bases, the relative importance of the CDVR quadrature errors rises quickly with increasing basis set size. This difference can be attributed to the change in the nature of the underlying dynamical pro-

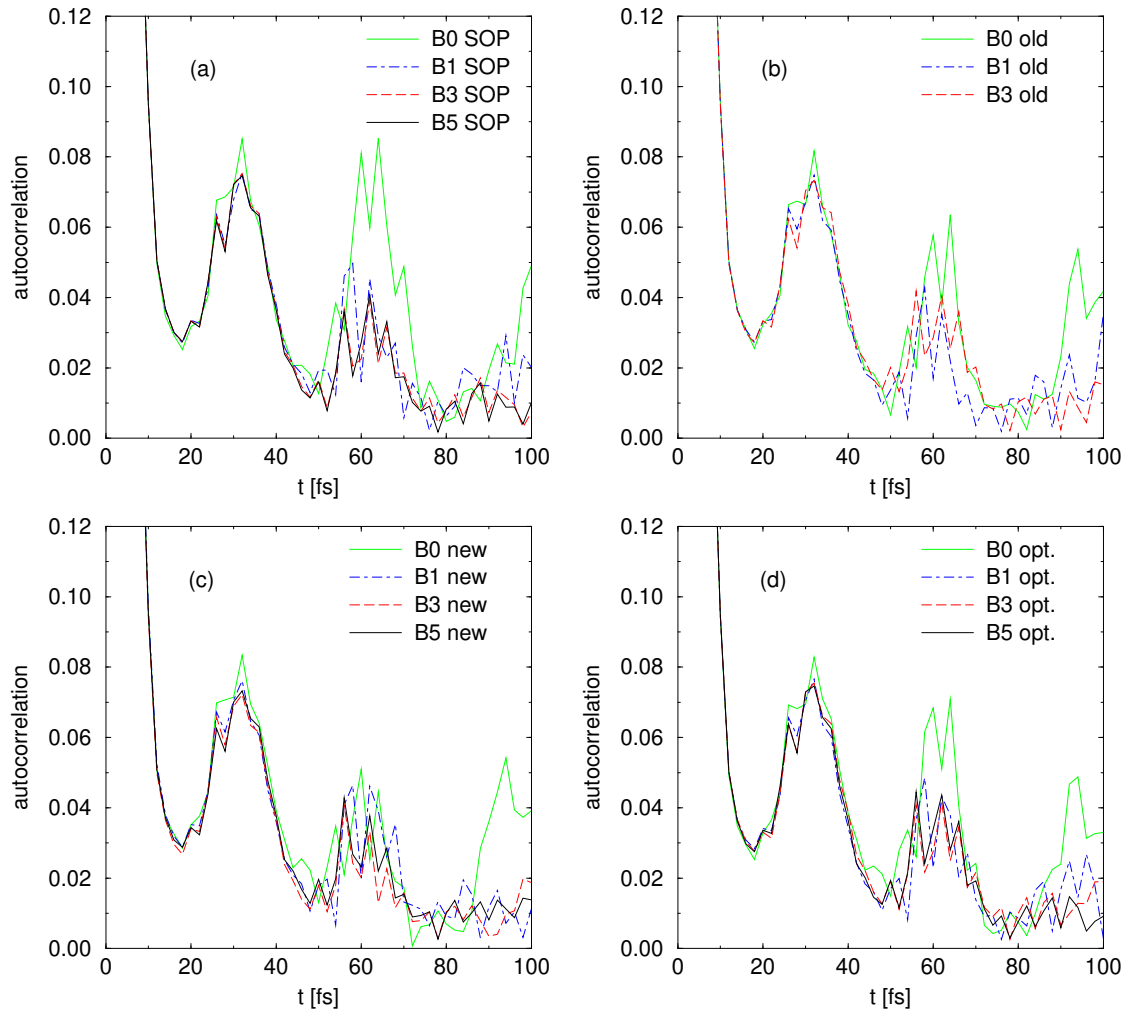


FIG. 4: The absolute values of the autocorrelation function obtained by different MCTDH calculations are displayed as a function of time. Panels (a) to (d) show results of MCTDH calculations using a SOP representation, the original non-hierarchical CDVR approach<sup>98,99</sup>, the revised non-hierarchical CDVR approach of the present work, and the revised non-hierarchical CDVR approach with optimized unoccupied SPFs (see text for details), respectively. Results obtained with different SPF basis sets size as indicated in the legend are displayed.

cesses. Initially, the wavepacket moves on the upper adiabatic PES. It shows a compact form and the CDVR approach can easily achieve an accurate quadrature. After 10 and 20 fs, the wavepacket passes from the upper to the lower adiabatic PES and starts fragmenting. Achieving an accurate quadrature for the increasingly delocalized and fragmented wavepacket is extremely demanding. Consequently, increasingly large differences between the SOP and CDVR results appear for SPF bases that cover the complex structure developing in the wavefunction in course of time.

Comparing the results computed with the original and the revised non-hierarchical CDVR displayed in panels (b) and (c) of Fig.3, only minor differences can be observed. The results obtained by the two approaches are essentially indistinguishable for the small basis sets B0 and B1. For the largest basis set shown in Fig.3b,

B3, the differences become notable. Here the calculations with the the original non-hierarchical CDVR yield slightly more accurate results. Results computed with the revised CDVR and the larger basis sets B4 and B5 are more accurate than the best results shown in panel (b). Due to the improved scaling of the revised CDVR, these calculations are numerically less demanding the calculations with the original non-hierarchical CDVR and basis set B3.

Improvements can be achieved if the unoccupied SPFs are replace by quadrature optimized SPFs as described in Sect.V. The results of these calculations are displayed in Fig.3d. For the small basis set B0 and B1, the results are essentially identical to the one displayed in panels (b) and (c). A relevant improvement compared to the calculations without quadrature optimized SPFs can be seen for the larger basis set B3, B4, and B5. For basis set B3,

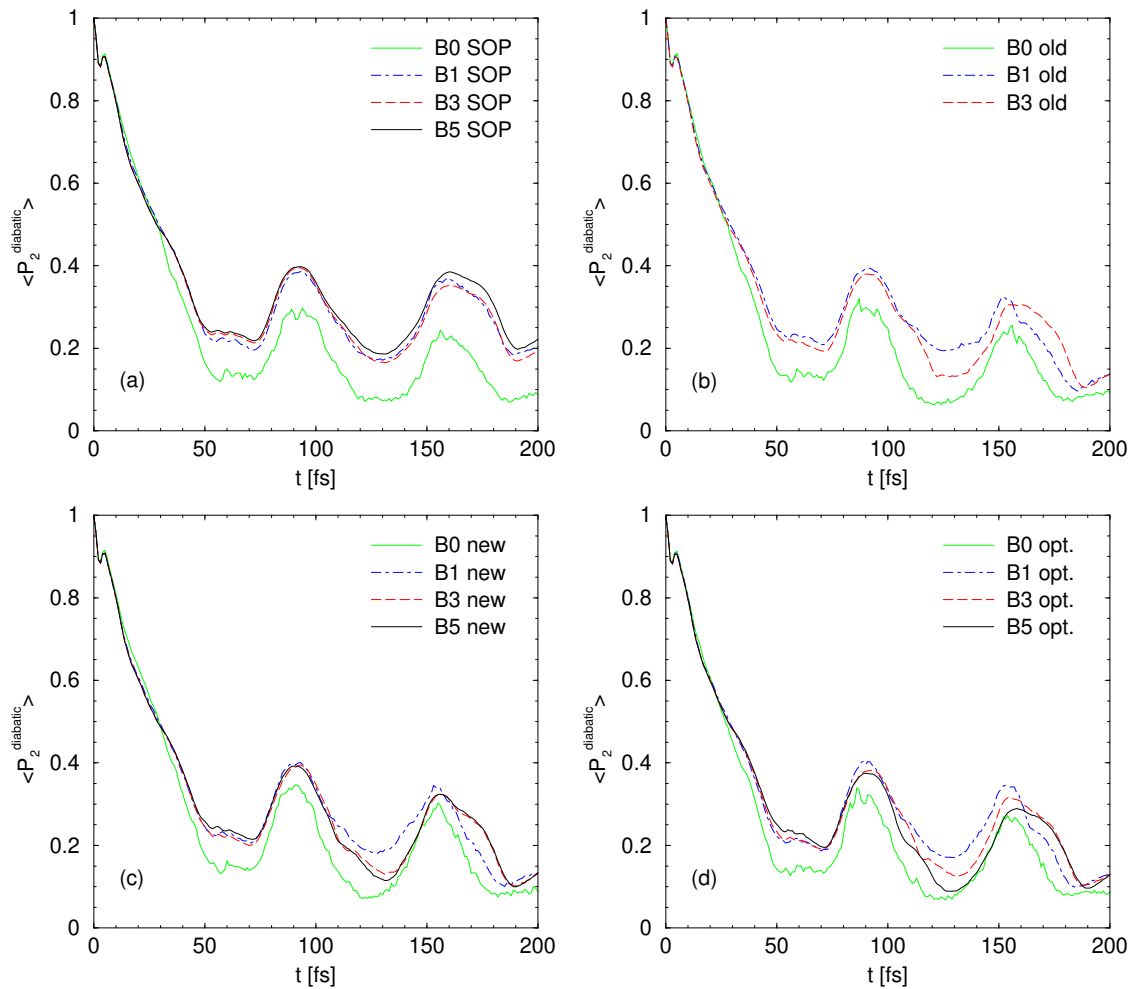


FIG. 5: The population of the second diabatic electronic state computed by different MCTDH calculations with different basis sets (indicated in the legend) is displayed as a function of time. Panels (a) to (d) show results of MCTDH calculations using a SOP representation, the original non-hierarchical CDVR approach<sup>98,99</sup>, the revised non-hierarchical CDVR approach of the present work, and the revised non-hierarchical CDVR approach with optimized unoccupied SPFs (see text for details), respectively. Results obtained with different SPF basis sets size as indicated in the legend are displayed.

the calculation using the revised CDVR and quadrature optimized SPFs are as accurate as the calculations with the original non-hierarchical CDVR.

As seen in Fig.3, it is extremely hard to achieve an accurate description of the entire wavefunction over the entire time scale considered. However, converged result can be obtained for many important physical observables as, e.g., the absorption spectrum or the population of the diabatic and adiabatic electronic states.

The autocorrelation function enables a detailed investigation of the various features appearing in the absorption spectrum. The absolute values of autocorrelation functions computed with the different approaches are shown in Fig.4. For any basis except the small B0 one, essentially converged results for times up to 50 fs are obtained using either the SOP or any of the CDVR schemes. Only for  $t > 50$  fs, appreciable difference between the CDVR and SOP calculations start to appear. Comparing the

results of different CVR schemes shown in panels (b) to (d), no relevant difference in the quality of the results can be observed.

The population of the second diabatic electronic state is investigated in Fig.5. Calculations utilizing the SOP form of the Hamiltonian achieve essentially converged results over the entire time interval for all but the smallest SPF bases (see panel (a)). All CDVR calculations provide similarly accurate results for times up to about 100 fs. For later times, the CDVR calculations are less accurate but provide a sound description of the population dynamics. Again, no relevant difference in the quality of the results obtained by the different CDVR schemes can be observed (see panel (b) to (d)).

An central advantage of the revised CDVR approach is the improved scaling with the numerical effort. As discussed in Sect.IV, the CPU time required by calculations using the revised CDVR,  $n$  SPF, and  $N$  configurations at

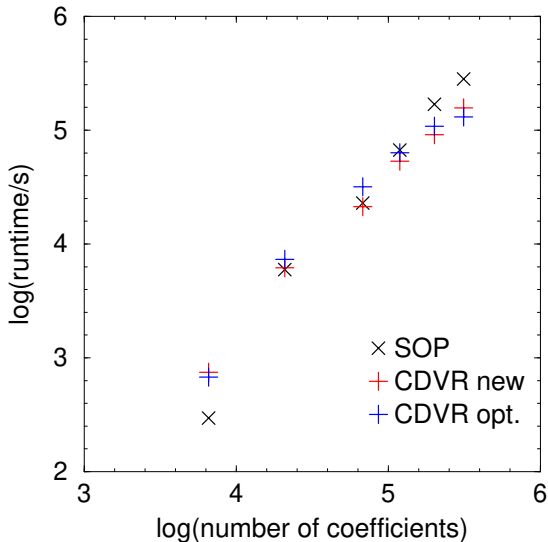


FIG. 6: Wall clock timings for calculations using the SOP scheme, the revised CDVR (CDVR new), and the revised CDVR with quadrature optimized SPFs (CDVR opt.) with different basis set sizes: the logarithm of the CPU time required is plotted versus the logarithm of the total number of A-coefficients used in the wavefunction representation. Results for basis set B0, B1, B2, B3, B4, and B5 are given. Note that in the figure a function  $y = const \cdot x^{4/3}$  would correspond to a line with a 45 degree slope.

a node ideally scales as  $n \cdot N$ . MCTDH calculations using a SOP-Hamiltonian show the same scaling of the numerical effort. For optimally structured tree where each node has three edges,  $N = n^3$ . Thus, the required CPU time should ideally scale as  $n^4 = N^{4/3}$ . However, indirect effects of the SPF basis set size, e.g., the dependence of the step sizes required in the integration scheme on the number of SPFs employed, can also affect the CPU time require and modify the scaling.

In Fig.6, the CPU times required by the different calculations considered above are analyzed. Results for MCTDH calculations with the basis sets B0, B1, B2, B3, B4, and B5 using the SOP form, the revised CDVR, and the revised CDVR and quadrature optimized SOPs are compared. Disregarding differences between the specific numbers of SPFs used at different edges, one would expect the CPU times should roughly scale as  $(total\ number\ of\ A\ coefficients)^{4/3}$ . The results shown in Fig.6 confirm this expectation for all types of calculations considered. Calculations using the revised CDVR do not scale worse than calculations utilizing the SOP form. (Actually, the revised CDVR calculation show a slightly more favorable scaling resulting from a slightly difference dependence of the step size in the integration on the SPF basis set size.)

Moreover, the absolute CPU times required by the different schemes for the same basis set are quite similar. Thus, the computational costs of the CDVR calculations are comparable to the SOP calculations. Considering

that the pyrazine system studied is ideally suited for MCTDH calculations using the SOP form, this result is remarkable and impressively demonstrates the numerical efficiency achieved by the revised CDVR approach.

Furthermore, the CPU times required for CDVR calculations with or without the use of quadrature optimized SPFs are roughly equal. For some basis sets, the calculations with quadrature optimized SPFs are faster than ones without. Thus, the effort for the computation of quadrature optimized SPFs is apparently irrelevant. Variations in integration steps sizes caused by the slight differences in the propagated wavefunction are more relevant for the numerical effort.

## VII. CONCLUSIONS AND OUTLOOK

The revised version of the non-hierarchical CDVR approach introduced in this work enables highly efficient multi-layer MCTDH calculations using general PESs of arbitrary structure. Compared to the original non-hierarchical CDVR approach, the revised scheme reduces the numerical effort while retaining the accuracy of quadrature. Calculations with the revised CDVR exhibit the same computational scaling with the size of the SPF basis sets as MCTDH calculations employing Hamiltonians in SOP form: for an ideally structure tree with three edges at each node and  $n$  SPF at each edge, the required CPU time scales as  $n^4$ . Furthermore, the revised CDVR approach eliminates artifacts resulting from the appearance of projections on the space spanned by the single-hole function present in the original version of the non-hierarchical CDVR.

Calculations studying the non-adiabatic dynamics of photoexcited pyrazine in full dimensionality (24D) impressively demonstrated the numerical efficiency of the revised non-hierarchical CDVR approach. Although this system is particularly well suited for MCTDH calculations exploiting the SOP structure of the diabatic potential, CDVR and SOP calculations require comparable CPU times. This result highlights the potential of the revised CDVR scheme for MCTDH calculations on complex ab initio PESs, where a SOP representation is not readily available.

Furthermore, a revised scheme for redefining unoccupied SPFs is introduced that systematically increases the accuracy of the CDVR quadrature without incurring significant additional computational cost. In principle, this approach enables systematic convergence of the quadrature to arbitrary accuracy.

Considering the numerical efficiency achieved by the revised non-hierarchical CDVR, interesting new lines of development could be envisioned. Employing on the fly-based techniques to obtain the potential energies on the sparse grids required by the non-hierarchical CDVR could be one direction. Growing SOP potentials based on the relevant potential energy values obtained by successive MCTDH calculations combining CDVR and SOP

representations of the potential are another option.

### Acknowledgments

The authors want to thank Hannes Hoppe for many stimulating discussions.

### Data availability

The data that supports the findings of this study is available within the article.

### Appendix A: Derivation of the optimal $\Delta\hat{V}_{t,rev}^{\lambda|\lambda_{0\kappa}}$

In the revised CDVR scheme, the action of the operator  $\Delta\hat{V}_t^{\lambda|\lambda_{0\kappa}}\hat{H}_t$  on the system's wavefunction is approximated by the action of the revised operator  $\Delta\hat{V}_{t,rev}^{\lambda|\lambda_{0\kappa}}\hat{H}_t$ . The optimal choice for  $\Delta\hat{V}_{t,rev}^{\lambda|\lambda_{0\kappa}}$  can be obtained by

$$\delta \left\| \left( \Delta\hat{V}_t^{\lambda|\lambda_{0\kappa}} - \Delta\hat{V}_{t,rev}^{\lambda|\lambda_{0\kappa}} \right) \hat{H}_t \Psi \right\|^2 = 0. \quad (53)$$

For hermitian  $\Delta\hat{V}_t^{\lambda|\lambda_{0\kappa}}$  and  $\Delta\hat{V}_{t,rev}^{\lambda|\lambda_{0\kappa}}$ , the variation with respect to  $\Delta\hat{V}_{t,rev}^{\lambda|\lambda_{0\kappa}}$  yields

$$\begin{aligned} 0 = & \delta \langle \hat{H}_t \Psi | - \Delta\hat{V}_t^{\lambda|\lambda_{0\kappa}} \delta \Delta\hat{V}_{t,ref}^{\lambda|\lambda_{0\kappa}} \\ & - \delta \Delta\hat{V}_{t,ref}^{\lambda|\lambda_{0\kappa}} \Delta\hat{V}_t^{\lambda|\lambda_{0\kappa}} \\ & + \Delta\hat{V}_{t,ref}^{\lambda|\lambda_{0\kappa}} \delta \Delta\hat{V}_t^{\lambda|\lambda_{0\kappa}} \\ & + \delta \Delta\hat{V}_{t,ref}^{\lambda|\lambda_{0\kappa}} \Delta\hat{V}_{t,ref}^{\lambda|\lambda_{0\kappa}} | \hat{H}_t \Psi \rangle. \end{aligned} \quad (54)$$

Varying

$$\Delta\hat{V}_{t,rev}^{\lambda|\lambda_{0\kappa}} = \sum_{i,j} |\xi_i^{\lambda|\lambda_{0\kappa}}\rangle \Delta\hat{V}_{t;ij}^{\lambda|\lambda_{0\kappa}} \langle \xi_j^{\lambda|\lambda_{0\kappa}}| \quad (55)$$

with respect to the  $\Delta\hat{V}_{t;ij}^{\lambda|\lambda_{0\kappa}}$ , the optimal  $\Delta\hat{V}_{t;ij}^{\lambda|\lambda_{0\kappa}}$  are thus given by

$$\begin{aligned} \langle \hat{H}_t \Psi | \Delta\hat{V}_t^{\lambda|\lambda_{0\kappa}} | \xi_i^{\lambda|\lambda_{0\kappa}} \rangle \langle \xi_j^{\lambda|\lambda_{0\kappa}} | \\ + | \xi_i^{\lambda|\lambda_{0\kappa}} \rangle \langle \xi_j^{\lambda|\lambda_{0\kappa}} | \Delta\hat{V}_t^{\lambda|\lambda_{0\kappa}} \\ - \Delta\hat{V}_{t,rev}^{\lambda|\lambda_{0\kappa}} | \xi_i^{\lambda|\lambda_{0\kappa}} \rangle \langle \xi_j^{\lambda|\lambda_{0\kappa}} | \\ - | \xi_i^{\lambda|\lambda_{0\kappa}} \rangle \langle \xi_j^{\lambda|\lambda_{0\kappa}} | \Delta\hat{V}_{t,rev}^{\lambda|\lambda_{0\kappa}} | \hat{H}_t \Psi \rangle = 0. \end{aligned} \quad (56)$$

Inserting the definitions of  $\Delta\hat{V}_t^{\lambda|\lambda_{0\kappa}}$  (see Eq.(31)) and  $\Delta\hat{V}_{t,rev}^{\lambda|\lambda_{0\kappa}}$ , the above equation can be rewritten as

$$\begin{aligned} \langle \hat{H}_t \Psi | \sum_{n,m,l} | \Xi_{nm}^{\lambda|\lambda_{0\kappa}} \rangle \Delta V_{t;nml}^{\lambda|\lambda_{0\kappa}} \langle \Xi_{jl}^{\lambda|\lambda_{0\kappa}} | \\ + \sum_{n,m,l} | \Xi_{il}^{\lambda|\lambda_{0\kappa}} \rangle \Delta V_{t;jlnm}^{\lambda|\lambda_{0\kappa}} \langle \Xi_{nm}^{\lambda|\lambda_{0\kappa}} | \\ - \sum_n | \xi_n^{\lambda|\lambda_{0\kappa}} \rangle \Delta V_{t,ni}^{\lambda|\lambda_{0\kappa}} \langle \xi_j^{\lambda|\lambda_{0\kappa}} | \\ - \sum_n | \xi_i^{\lambda|\lambda_{0\kappa}} \rangle \Delta V_{t,jn}^{\lambda|\lambda_{0\kappa}} \langle \xi_n^{\lambda|\lambda_{0\kappa}} | \hat{H}_t \Psi \rangle = 0. \end{aligned} \quad (57)$$

With the definitions introduced in Eqs.(36) and (37), one finds

$$\begin{aligned} 0 = & X_{t;ji}^{\lambda|\lambda_{0\kappa}*} + X_{t;ij}^{\lambda|\lambda_{0\kappa}} \\ & - \sum_{n,m} u_{t;nm}^{\lambda|\lambda_{0\kappa}} r_{t;m}^{\lambda|\lambda_{0\kappa}} u_{t;jm}^{\lambda|\lambda_{0\kappa}*} \cdot \Delta V_{t,ni}^{\lambda|\lambda_{0\kappa}} \\ & - \sum_{n,m} u_{t;im}^{\lambda|\lambda_{0\kappa}} r_{t;m}^{\lambda|\lambda_{0\kappa}} u_{t;nm}^{\lambda|\lambda_{0\kappa}*} \cdot \Delta V_{t,jn}^{\lambda|\lambda_{0\kappa}}. \end{aligned} \quad (58)$$

Since the  $u_t^{\lambda|\lambda_{0\kappa}}$  are unitary matrices, multiplication with  $u_{t;ia}^{\lambda|\lambda_{0\kappa}*} u_{t;jb}^{\lambda|\lambda_{0\kappa}}$  and summation over  $i$  and  $j$  yields

$$\begin{aligned} 0 = & \sum_{i,j} u_{t;ia}^{\lambda|\lambda_{0\kappa}*} u_{t;jb}^{\lambda|\lambda_{0\kappa}} \cdot \left( X_{t;ji}^{\lambda|\lambda_{0\kappa}*} + X_{t;ij}^{\lambda|\lambda_{0\kappa}} \right) \\ & - \sum_{n,i} u_{t;nb}^{\lambda|\lambda_{0\kappa}} r_{t;b}^{\lambda|\lambda_{0\kappa}} u_{t;ia}^{\lambda|\lambda_{0\kappa}*} \cdot \Delta V_{t,ni}^{\lambda|\lambda_{0\kappa}} \\ & - \sum_{n,j} u_{t;jb}^{\lambda|\lambda_{0\kappa}} r_{t;a}^{\lambda|\lambda_{0\kappa}} u_{t;na}^{\lambda|\lambda_{0\kappa}*} \cdot \Delta V_{t,jn}^{\lambda|\lambda_{0\kappa}}. \end{aligned} \quad (59)$$

Relabeling the summation indices, the two last terms can be combined:

$$\begin{aligned} 0 = & \sum_{k,l} u_{t;ka}^{\lambda|\lambda_{0\kappa}*} u_{t;lb}^{\lambda|\lambda_{0\kappa}} \cdot \left( X_{t;lk}^{\lambda|\lambda_{0\kappa}*} + X_{t;kl}^{\lambda|\lambda_{0\kappa}} \right) \\ & - \left( r_{t;a}^{\lambda|\lambda_{0\kappa}} + r_{t;b}^{\lambda|\lambda_{0\kappa}} \right) \sum_{n,m} u_{t;nb}^{\lambda|\lambda_{0\kappa}} u_{t;ma}^{\lambda|\lambda_{0\kappa}*} \Delta V_{t,nm}^{\lambda|\lambda_{0\kappa}}. \end{aligned} \quad (60)$$

The final result given in the main part of the article, Eq.(35), is then obtained by multiplication with

$$\frac{u_{t;ib}^{\lambda|\lambda_{0\kappa}*} u_{t;ja}^{\lambda|\lambda_{0\kappa}}}{r_{t;a}^{\lambda|\lambda_{0\kappa}} + r_{t;b}^{\lambda|\lambda_{0\kappa}}} \quad (61)$$

and summation over  $a$  and  $b$ .

### Appendix B: Separable potentials

For separable potentials, the quadrature provided by the revised CDVR is accurate even if the SPF basis set

sizes are not converged. To prove this feature, it is sufficient to prove that the revised CDVR is accurate for potentials that dependent only on a single coordinate: since the CDVR potential operator is a linear function of the potential, the revised CDVR describes a sum of potentials correctly if each term in the sum is described correctly.

Now we consider a potential  $V_t$  that depends only a single coordinate present in the coordinate set  $q^\lambda$  associated with the node ( $\lambda$ ) and investigate the potential corrections  $\Delta \hat{V}_{t,rev}^{\lambda \circ \kappa | \lambda}$ . Since the potential depends only on  $q^\lambda$ ,  $\hat{V}_{t,\kappa}^\lambda$  does not act on  $|\xi_l^{\lambda \circ \kappa | \lambda}\rangle$  and  $V_t(\Xi_{k,i}^{\lambda \circ \kappa | \lambda}) = V_t(\xi_k^{\lambda \circ \kappa | \lambda})$ . Then the  $X_{t;lk}^{\lambda \circ \kappa | \lambda}$  in Eq.40 can be simplified:

$$\begin{aligned} X_{t;lk}^{\lambda \circ \kappa | \lambda} &= -\langle \Psi | \xi_l^{\lambda \circ \kappa | \lambda} \rangle V_t(\xi_k^{\lambda \circ \kappa | \lambda}) \langle \xi_k^{\lambda \circ \kappa | \lambda} | \Psi \rangle \\ &\quad + \langle \Psi | \xi_l^{\lambda \circ \kappa | \lambda} \rangle \sum_n \sum_I \langle \xi_k^{\lambda \circ \kappa | \lambda} | \Xi_I^\lambda \rangle \\ &\quad \cdot \langle \Xi_I^\lambda | \hat{V}_{t,\kappa}^\lambda | \xi_n^{\lambda \circ \kappa | \lambda} \rangle \langle \xi_n^{\lambda \circ \kappa | \lambda} | \Psi \rangle \\ &= \sum_n \langle \Psi | \xi_l^{\lambda \circ \kappa | \lambda} \rangle \langle \xi_n^{\lambda \circ \kappa | \lambda} | \Psi \rangle \\ &\quad \cdot \langle \xi_k^{\lambda \circ \kappa | \lambda} | -V_t(\xi_k^{\lambda \circ \kappa | \lambda}) + \hat{V}_{t,\kappa}^\lambda | \xi_n^{\lambda \circ \kappa | \lambda} \rangle \\ &= \sum_{n,m} u_{t;lm}^{\lambda \circ \kappa | \lambda} \cdot r_{t;m}^{\lambda \circ \kappa | \lambda} \cdot u_{t;nm}^{\lambda \circ \kappa | \lambda *} \\ &\quad \cdot \langle \xi_k^{\lambda \circ \kappa | \lambda} | -V_t(\xi_k^{\lambda \circ \kappa | \lambda}) + \hat{V}_{t,\kappa}^\lambda | \xi_n^{\lambda \circ \kappa | \lambda} \rangle. \quad (62) \end{aligned}$$

Analogously, one finds

$$\begin{aligned} X_{t;kl}^{\lambda \circ \kappa | \lambda *} &= \sum_{n,m} u_{t;nm}^{\lambda \circ \kappa | \lambda} \cdot r_{t;m}^{\lambda \circ \kappa | \lambda} \cdot u_{t;km}^{\lambda \circ \kappa | \lambda *} \\ &\quad \cdot \langle \xi_n^{\lambda \circ \kappa | \lambda} | -V_t(\xi_l^{\lambda \circ \kappa | \lambda}) + \hat{V}_{t,\kappa}^\lambda | \xi_l^{\lambda \circ \kappa | \lambda} \rangle. \quad (63) \end{aligned}$$

These two results can be combined to obtain

$$\begin{aligned} C_{t;ij}^{\lambda \circ \kappa | \lambda} &= \sum_{l,k} u_{t;li}^{\lambda \circ \kappa | \lambda *} \cdot u_{t;kj}^{\lambda \circ \kappa | \lambda} \cdot (X_{t;kl}^{\lambda \circ \kappa | \lambda *} + X_{t;lk}^{\lambda \circ \kappa | \lambda}) \\ &= \sum_{n,l} u_{t;nj}^{\lambda \circ \kappa | \lambda} \cdot r_{t;j}^{\lambda \circ \kappa | \lambda} \cdot u_{t;li}^{\lambda \circ \kappa | \lambda *} \\ &\quad \cdot \langle \xi_n^{\lambda \circ \kappa | \lambda} | -V_t(\xi_l^{\lambda \circ \kappa | \lambda}) + \hat{V}_{t,\kappa}^\lambda | \xi_l^{\lambda \circ \kappa | \lambda} \rangle \\ &\quad + \sum_{n,k} u_{t;kj}^{\lambda \circ \kappa | \lambda} \cdot r_{t;i}^{\lambda \circ \kappa | \lambda} \cdot u_{t;ni}^{\lambda \circ \kappa | \lambda *} \\ &\quad \cdot \langle \xi_k^{\lambda \circ \kappa | \lambda} | -V_t(\xi_k^{\lambda \circ \kappa | \lambda}) + \hat{V}_{t,\kappa}^\lambda | \xi_n^{\lambda \circ \kappa | \lambda} \rangle \\ &= \sum_{n,m} u_{t;mj}^{\lambda \circ \kappa | \lambda} \cdot (r_{t;i}^{\lambda \circ \kappa | \lambda} + r_{t;j}^{\lambda \circ \kappa | \lambda}) \cdot u_{t;ni}^{\lambda \circ \kappa | \lambda *} \\ &\quad \cdot \langle \xi_m^{\lambda \circ \kappa | \lambda} | -V_t(\xi_m^{\lambda \circ \kappa | \lambda}) + \hat{V}_{t,\kappa}^\lambda | \xi_n^{\lambda \circ \kappa | \lambda} \rangle \quad (64) \end{aligned}$$

Inserting this result into Eq.35, the final result for the potential correction matrix reads

$$\Delta V_{t;ij}^{\lambda \circ \kappa | \lambda} = \langle \xi_i^{\lambda \circ \kappa | \lambda} | -V_t(\xi_i^{\lambda \circ \kappa | \lambda}) + \hat{V}_{t,\kappa}^\lambda | \xi_j^{\lambda \circ \kappa | \lambda} \rangle. \quad (65)$$

Consequently, the operator associated with the potential correction is the revised CDVR for a potential depending only on  $q^\lambda$ ,

$$\Delta \hat{V}_{t,rev}^{\lambda \circ \kappa | \lambda} = -\hat{V}_t^{\lambda \circ \kappa | \lambda} + \hat{V}_{t,\kappa}^\lambda, \quad (66)$$

correctly compensates for all errors resulting from the use of the scarce grid  $\Xi_N^{\lambda \circ \kappa}$  at node ( $\lambda \circ \kappa$ ).

- <sup>1</sup> H.-D. Meyer, U. Manthe, and L. S. Cederbaum, Chem. Phys. Lett. **165**, 73 (1990).
- <sup>2</sup> U. Manthe, H.-D. Meyer, and L. S. Cederbaum, J. Chem. Phys. **97**, 3199 (1992).
- <sup>3</sup> H. Wang and M. Thoss, J. Chem. Phys. **119**, 1289 (2003).
- <sup>4</sup> U. Manthe, J. Chem. Phys. **128**, 164116 (2008).
- <sup>5</sup> E. Y. Wilner, H. Wang, M. Thoss, and E. Rabani, Phys. Rev. B **89**, 205129 (2014).
- <sup>6</sup> K. Balzer, Z. Li, O. Vendrell, and M. Eckstein, Phys. Rev. B **91**, 045136 (2015).
- <sup>7</sup> M. Schroeter and O. Kuehn, J. Phys. Chem. A **117**, 7580 (2013).
- <sup>8</sup> S. Lopez-Lopez, R. Martinazzo, and M. Nest, J. Chem. Phys. **134**, 094102 (2011).
- <sup>9</sup> T. Westermann, R. Brodbeck, A. B. Rozhenko, W. W. Schoeller, and U. Manthe, J. Chem. Phys. **135**, 184102 (2011).
- <sup>10</sup> F. Bouakline, F. Lueder, R. Martinazzo, and P. Saalfrank, J. Phys. Chem. A **116**, 11118 (2012).
- <sup>11</sup> L. Uranga-Pina, C. Meier, and J. Rubayo-Soneira, Chem. Phys. Lett. **543**, 12 (2012).

- <sup>12</sup> M. Moix Teixidor and F. Huarte-Larranaga, Chem. Phys. **399**, 264 (2012).
- <sup>13</sup> V. S. Reddy, C. Camacho, J. Xia, R. Jasti, and S. Irle, J. Chem. Theo. Comp. **10**, 4025 (2014).
- <sup>14</sup> W. Eisfeld, O. Vieuxmaire, and A. Viel, J. Chem. Phys. **140**, 224109 (2014).
- <sup>15</sup> A. Valdes and R. Prosimiti, J. Phys. Chem. A **117**, 9518 (2013).
- <sup>16</sup> D. Skouteris and A. Lagana, Chem. Phys. Lett. **575**, 18 (2013).
- <sup>17</sup> B. Zhao, D.-H. Zhang, S.-Y. Lee, and Z. Sun, J. Chem. Phys. **140**, 164108 (2014).
- <sup>18</sup> J. Schulze, M. F. Shibl, M. J. Al-Marri, and O. Kühn, J. Chem. Phys. **144**, 185101 (2016).
- <sup>19</sup> D. M. G. Williams, W. Eisfeld, and A. Viel, Phys. Chem. Chem. Phys. **24**, 24706 (2022).
- <sup>20</sup> S. Han, M. Schroeder, F. Gatti, H.-D. Meyer, D. Lauvergnat, D. R. Yarkony, and H. Guo, J. Chem. Theory Comput. **18**, 4627 (2022).
- <sup>21</sup> A. B. Trofimov, A. D. Skitnevskaya, E. K. Grigorieva, E. Gromov, V. and H. Koppel, J. Chem. Phys. **157**,

- 174309 (2022).
- 22 S. V. K. Isukapalli and S. R. Vennapusa, *J. Photochem. Photobiol. A-Chem.* **441**, 114695 (2023).
  - 23 H. Tajouo Tela, E. Quintas-Sanchez, M.-L. Dubernet, Y. Scribano, R. Dawes, F. Gatti, and S. Ndengue, *Phys. Chem. Chem. Phys.* **25**, 31813 (2023).
  - 24 T. Niermann, H. Hoppe, and U. Manthe, *J. Chem. Phys.* **161**, 134109 (2024).
  - 25 D. Brey and I. Burghardt, *J. Phys. Chem. Lett.* **15**, 1836 (2024).
  - 26 V. J. Rani, A. K. Kanakati, and S. Mahapatra, *J. Chem. Phys.* **161**, 094302 (2024).
  - 27 L. Shi, M. Schroeder, H.-D. Meyer, D. e. Pelaez, A. M. Wodtke, K. Golibrzuch, A.-M. Schoenemann, A. Kandratsenka, and F. Gatti, *J. Phys. Chem. A* **129**, 1896 (2025).
  - 28 A. Dubey, Z. Zeybek, F. Kohler, R. Mukherjee, and P. Schmelcher, *Phys. Rev. Res.* **7**, 023039 (2025).
  - 29 S. Ray, S. Sasmal, and P. Mondal, *J. Chem. Phys.* **163**, 144310 (2025).
  - 30 F. Huarte-Larrañaga and U. Manthe, *J. Chem. Phys.* **113**, 5115 (2000).
  - 31 F. Huarte-Larrañaga and U. Manthe, *J. Phys. Chem. A* **105**, 2522 (2001).
  - 32 T. Wu, H.-J. Werner, and U. Manthe, *Science* **306**, 2227 (2004).
  - 33 R. van Harrevelt, G. Nyman, and U. Manthe, *J. Chem. Phys.* **126**, 084303 (2007).
  - 34 G. Nyman, R. van Harrevelt, and U. Manthe, *J. Phys. Chem. A* **111**, 10331 (2007).
  - 35 R. Welsch and U. Manthe, *J. Chem. Phys.* **141**, 051102 (2014).
  - 36 R. Welsch and U. Manthe, *J. Chem. Phys.* **141**, 174313 (2014).
  - 37 R. Welsch and U. Manthe, *J. Chem. Phys.* **142**, 064309 (2015).
  - 38 R. Ellerbrock and U. Manthe, *Chem. Phys.* **482**, 106 (2017).
  - 39 R. Welsch and U. Manthe, *J. Phys. Chem. Lett.* **6**, 338 (2015).
  - 40 R. Ellerbrock and U. Manthe, *J. Chem. Phys.* **147**, 241104 (2017).
  - 41 R. Ellerbrock and U. Manthe, *J. Chem. Phys.* **148**, 224303 (2018).
  - 42 R. Ellerbrock and U. Manthe, *Faraday Discussions* **212**, 217 (2018).
  - 43 B. Zhao and U. Manthe, *J. Chem. Phys.* **150**, 184103 (2019).
  - 44 H. Hoppe and U. Manthe, *J. Phys. Chem. Lett.* **13**, 2563 (2022).
  - 45 M. D. Coutinho-Neto, A. Viel, and U. Manthe, *J. Chem. Phys.* **121**, 9207 (2004).
  - 46 T. Hammer, M. D. Coutinho-Neto, A. Viel, and U. Manthe, *J. Chem. Phys.* **131**, 224109 (2009).
  - 47 T. Hammer and U. Manthe, *J. Chem. Phys.* **134**, 224305 (2011).
  - 48 M. Schroeder, F. Gatti, and H.-D. Meyer, *J. Chem. Phys.* **134**, 234307 (2011).
  - 49 T. Hammer and U. Manthe, *J. Chem. Phys.* **136**, 054105 (2012).
  - 50 M. Schroeder and H.-D. Meyer, *J. Chem. Phys.* **141**, 034116 (2014).
  - 51 O. Vendrell, F. Gatti, and H.-D. Meyer, *Angew. Chemie Int. Ed.* **46**, 6918 (2007).
  - 52 O. Vendrell, F. Gatti, D. Lauvergnat, and H.-D. Meyer, *J. Chem. Phys.* **127**, 184302 (2007).
  - 53 O. Vendrell, F. Gatti, and H.-D. Meyer, *J. Chem. Phys.* **127**, 184303 (2007).
  - 54 O. Vendrell, M. Brill, F. Gatti, and H.-D. Meyer, *J. Chem. Phys.* **130**, 234305 (2009).
  - 55 O. Vendrell, F. Gatti, and H.-D. Meyer, *J. Chem. Phys.* **131**, 034308 (2009).
  - 56 H. R. Larsson, M. Schroeder, R. Beckmann, F. Briec, C. Schran, D. Marx, and O. Vendrell, *Chem. Sci.* **13**, 11119 (2022).
  - 57 M. Schroeder, F. Gatti, D. Lauvergnat, H.-D. Meyer, and O. Vendrell, *Nat. Comm.* **13**, 6170 (2022).
  - 58 G. A. Worth, H.-D. Meyer, and L. S. Cederbaum, *J. Chem. Phys.* **105**, 4412 (1996).
  - 59 G. A. Worth, H.-D. Meyer, and L. S. Cederbaum, *J. Chem. Phys.* **109**, 3518 (1998).
  - 60 A. Raab, G. A. Worth, H.-D. Meyer, and L. S. Cederbaum, *J. Chem. Phys.* **110**, 936 (1999).
  - 61 H. Wang, D. E. Skinner, and M. Thoss, *J. Chem. Phys.* **125**, 174502 (2006).
  - 62 I. Kondov, M. Cizek, C. Benesch, M. Thoss, and H. Wang, *J. Phys. Chem. C* **111**, 11970 (2007).
  - 63 H. Wang, I. Pshenichnyuk, R. Härtle, and M. Thoss, *J. Chem. Phys.* **135**, 244506 (2011).
  - 64 M. Beck, A. Jäckle, G. A. Worth, and H.-D. Meyer, *Physics Reports* **324**, 1 (2000).
  - 65 H.-D. Meyer and G. A. Worth, *Theor. Chem. Acc.* **109**, 251 (2003).
  - 66 F. Huarte-Larrañaga and U. Manthe, *Z. Phys. Chem.* **221**, 171 (2007).
  - 67 G. A. Worth, H. D. Meyer, H. Koeppl, L. S. Cederbaum, and I. Burghardt, *Int. Rev. Phys. Chem.* **27**, 569 (2008).
  - 68 H.-D. Meyer, F. Gatti, and G. A. Worth, *Multidimensional Quantum Dynamics: MCTDH Theory and Applications* (Weinheim: Wiley-VCH, 2009).
  - 69 H.-D. Meyer, *Wiley Interdisciplinary Reviews: Computational Molecular Science* **2**, 351 (2012).
  - 70 H. Wang, *J. Phys. Chem. A* **119**, 7951 (2015).
  - 71 U. Manthe, *J. Phys.:Condens. Matter* **29**, 253001 (2017).
  - 72 A. Jäckle and H.-D. Meyer, *J. Chem. Phys.* **104**, 7974 (1996).
  - 73 A. Jäckle and H.-D. Meyer, *J. Chem. Phys.* **109**, 3772 (1998).
  - 74 D. Pelaez and H.-D. Meyer, *J. Chem. Phys.* **138**, 014108 (2013).
  - 75 F. Otto, *J. Chem. Phys.* **140**, 014106 (2014).
  - 76 M. Schroeder and H.-D. Meyer, *J. Chem. Phys.* **147**, 064105 (2017).
  - 77 M. Schroeder, *J. Chem. Phys.* **152**, 024108 (2020).
  - 78 U. Manthe, *J. Chem. Phys.* **105**, 6989 (1996).
  - 79 R. van Harrevelt und U. Manthe, *J. Chem. Phys.* **121**, 5623 (2004).
  - 80 R. van Harrevelt and U. Manthe, *J. Chem. Phys.* **123**, 064106 (2005).
  - 81 U. Manthe, *J. Chem. Phys.* **130**, 054109 (2009).
  - 82 F. Huarte-Larrañaga and U. Manthe, *J. Chem. Phys.* **116**, 2863 (2002).
  - 83 F. Huarte-Larrañaga and U. Manthe, *J. Chem. Phys.* **117**, 4635 (2002).
  - 84 G. Schiffel and U. Manthe, *J. Chem. Phys.* **132**, 084103 (2010).
  - 85 T. Westermann, J. B. Kim, M. L. Weichman, C. Hock, T. I. Yacovitch, J. Palma, D. M. Neumark, and U. Man-

- the, *Angew. Chem. Int. Ed.* **53**, 1122 (2014).
- <sup>86</sup> D. Schäpers and U. Manthe, *J. Phys. Chem. A* **120**, 3186 (2016).
- <sup>87</sup> D. Schäpers and U. Manthe, *J. Chem. Phys.* **151**, 104106 (2019).
- <sup>88</sup> R. Wodraszka and T. Carrington, *J. Chem. Phys.* **148**, 044115 (2018).
- <sup>89</sup> R. Wodraszka and T. Carrington, *J. Chem. Phys.* **150**, 154108 (2019).
- <sup>90</sup> R. Wodraszka and T. Carrington, *J. Chem. Phys.* **152**, 164117 (2020).
- <sup>91</sup> R. Wodraszka and T. Carrington, *J. Chem. Phys.* **154**, 114107 (2021).
- <sup>92</sup> S. A. Smolyak, *Sov. Math. Dokl.* **4**, 240 (1963).
- <sup>93</sup> G. Avila and T. Carrington, Jr., *J. Chem. Phys.* **131**, 174103 (2009).
- <sup>94</sup> G. Avila and T. Carrington, Jr., *J. Chem. Phys.* **134**, 054126 (2011).
- <sup>95</sup> C. Lubich, *Appl. Math. Res. Express* , 311 (2015).
- <sup>96</sup> H. R. Larsson, *J. Chem. Phys.* **151**, 204102 (2019).
- <sup>97</sup> T. Weike and U. Manthe, *J. Chem. Phys.* **154**, 194108 (2021).
- <sup>98</sup> R. Ellerbrock and U. Manthe, *J. Chem. Phys.* **156**, 134107 (2022).
- <sup>99</sup> R. Ellerbrock, H. Hoppe, and U. Manthe, *J. Chem. Phys.* **160**, 224108 (2024).
- <sup>100</sup> R. Ellerbrock, H. Hoppe, and U. Manthe, *J. Chem. Phys.* **158**, 244103 (2023).
- <sup>101</sup> A. Viel, W. Eisfeld, S. Neumann, W. Domcke, and U. Manthe, *J. Chem. Phys.* **124**, 214306 (2006).
- <sup>102</sup> M. H. Beck and H.-D. Meyer, *Z. Phys. D* **42**, 113 (1997).
- <sup>103</sup> U. Manthe, *Chem. Phys.* **329**, 168 (2006).
- <sup>104</sup> R. Schinke, M. Nonella, H. Suter, and J. Huber, *J. Chem. Phys.* **93**, 1098 (1990).
- <sup>105</sup> U. Manthe, *J. Chem. Phys.* **128**, 064108 (2008).
- <sup>106</sup> C. Evenhuis, G. Nyman, and U. Manthe, *J. Chem. Phys.* **127**, 144302 (2007).
- <sup>107</sup> D. M. Medvedev, L. B. Harding, and S. K. Gray, *Molecular Physics* **104**, 73 (2006).
- <sup>108</sup> R. Schneider and W. Domcke, *Chem. Phys. Lett.* **150**, 235 (1988).
- <sup>109</sup> R. Schneider, W. Domcke, and H. Köppel, *J. Chem. Phys.* **92**, 1045 (1990).
- <sup>110</sup> L. Seidner, G. Stock, A. L. Sobolewski, and W. Domcke, *J. Chem. Phys.* **96**, 5298 (1992).
- <sup>111</sup> C. Woywood, W. Domcke, A. L. Sobolewski, and H.-J. Werner, *J. Chem. Phys.* **100**, 1400 (1994).
- <sup>112</sup> U. Manthe and H. Köppel, *J. Chem. Phys.* **93**, 1658 (1990).
- <sup>113</sup> S. Krempel, M. Winterstetter, H. Plöhn, and W. Domcke, *J. Chem. Phys.* **100**, 926 (1994).
- <sup>114</sup> S. Krempel, M. Winterstetter, H. Plöhn, and W. Domcke, *J. Chem. Phys.* **102**, 6499 (1995).
- <sup>115</sup> O. Vendrell and H.-D. Meyer, *J. Chem. Phys.* **134**, 044135 (2011).
- <sup>116</sup> T. Westermann and U. Manthe, *J. Chem. Phys.* **137**, 22A509 (2012).